Defining the spectral characteristics of rocks within the Mambulu Complex, Natal Belt, South Africa

Zayd Goolam Hoosen

204513803

Submitted in fulfilment of the academic requirements for the degree of
Master of Science in the School of Agricultural, Earth and Environmental Sciences,
College of Agriculture, Engineering and Science,
University of KwaZulu-Natal
Durban

November 2012

As the candidate's supervisor I have/have not approved this thesis/dissertation for submission.

Signed: _____   Name: _____   Date: _____

PREFACE

The work undertaken in this study was carried out at School of Agricultural, Earth and Environmental Sciences, College of Agriculture, Engineering and Science, University of KwaZulu-Natal, Durban. This research was completed under the supervision of the following academic staff:

Professor S. McCourt, School of Agricultural, Earth and Environmental Sciences, College of Agriculture, Engineering and Science, University of KwaZulu-Natal, Durban.

Professor F.B. Ahmed, formerly of the School of Agricultural, Earth and Environmental Sciences, College of Agriculture, Engineering and Science, University of KwaZulu-Natal, now at the University of Johannesburg.

The duration of this study was from July 2009 to November 2012.

The contents of this work have not been submitted in any form to another University and, except where the work of others is acknowledged in the text, the results are the author's own investigation.

———————————————

Zayd Goolam Hoosen

November 2012

We certify that the above statement is correct:

———————————————   ———————————————

Professor. S. McCourt   Professor. F.B. Ahmed

COLLEGE OF AGRICULTURE, ENGINEERING AND SCIENCE

DECLARATION 1 - PLAGIARISM

I, Zayd Goolam Hoosen, declare that

1. The research reported in this thesis, except where otherwise indicated, is my original research.

2. This thesis has not been submitted for any degree or examination at any other university.

3. This thesis does not contain other persons' data, pictures, graphs or other information, unless specifically acknowledged as being sourced from other persons.

4. This thesis does not contain other persons' writing, unless specifically acknowledged as being sourced from other researchers. Where other written sources have been quoted, then:

a. Their words have been re-written but the general information attributed to them has been referenced
b. Where their exact words have been used, then their writing has been placed in italics and inside quotation marks, and referenced.

5. This thesis does not contain text, graphics or tables copied and pasted from the Internet, unless specifically acknowledged, and the source being detailed in the thesis and in the References sections.

Signed……………………………………………………………………………

CMC Feb 2012

TABLE OF CONTENTS

CHAPTER ONE

1. INTRODUCTION AND PROBLEM CONTEXTUALISATION

CHAPTER TWO

2. FIELD SPECTROSCOPY AND ITS GEOLOGICAL APPLICATIONS

CHAPTER THREE

3. STUDY AREA AND METHODOLOGY

CHAPTER FOUR

4. RESULTS AND DISCUSSION

CHAPTER FIVE

5. RECOMMENDATIONS AND CONCLUSIONS

LIST OF FIGURES

LIST OF PLATES

LIST OF TABLES

LIST OF ABBREVIATIONS

%	Percentage
°	Degree
°C	Degree Centigrade
°S	Degree South
°E	Degree East
~	Approximately
≡	Identical To
μm	Micrometer
Al	Aluminium
An	Anorthite
Ca	Calcium
cm	Centimetre
cm^{-1}	Reciprocal Centimetre
CO_3^{2-}	Carbonate
E	Emmittance
Fe	Iron
Fe^{2+}	Ferrous Iron
Fe^{3+}	Ferric Iron
FeO	Iron Oxide
Ga	Billion Years Ago
H_2O	Water
Km	Kilometre
m	Metre
m^2	Square Metre
Ma	Million Years Ago
Mg	Magnesium
mm	Millimetre

Ni	Nickel
nm	Nanometre
OH	Hydroxyl
R	Reflectance
SiO_4^{4-}	Silicate
str	Steradian
Ti	Titanium
W	Watt

LIST OF ACRONYMS

ANOVA	Analysis of Variance
ASD	Analytical Spectral Devices
AVIRIS	Airborne Visible Infrared Imaging Spectrometer
BRDF	Bidirectional Reflectance Distribution Function
ENVI	Environment for Visualising Images
FIFE	First ISLSCP Field Experiment
HySI	Hyperspectral Imager
IFOV	Instantaneous Field of View
IR	Infrared
ISLSCP	International Satellite Land Surface Climatology Project
JHU	Johns Hopkins University
JPL	Jet Propulsion Laboratory
KZN	KwaZulu-Natal
MS	Microsoft
NIR	Near-Infrared
PIDAS	Portable Instant Display and Analysis Spectrometer
SPSS	Statistical Package for the Social Sciences
UKZN	University of KwaZulu-Natal
UV	Ultraviolet

ABSTRACT

Field and laboratory spectroscopy are sub-fields of remote sensing, where the radiometric data of materials are individually measured either where the materials occur *in situ* or in a controlled laboratory environment. Both applications require the use of a spectroradiometer to record this reflected electromagnetic radiation. The spectral properties of rocks from the Mambulu Complex in the Natal Belt have not been studied previously. Four dominant rock types, namely, massif-type anorthosite, leuco-gabbro, pyroxenite and magnetitite were sampled from the Mambulu Complex and their spectral reflectances measured. Absorption features were determined after continuum removal was applied to the spectra.

Anorthosite showed absorption features at 480-490, 592, 603, 608, 627-726, 765, 1410, 1905-1955, 2200, 2250 and 2330nm. For leuco-gabbro absorption features were observed at 481, 950-1010, 1407, 1917, 2206, 2252, and 2300-2340nm. Magnetitite displayed absorption features at 414, 460-515, 620-715, 982, 1380-1480, 1800, 1905-1930 and 2145-2330nm. For medium-grained pyroxenite absorption features were present at 410-420, 483, 680, 977-993, 1410-1415, 1800, 1920, 2205, 2250, 2307, 2400 and 2430nm. Coarse-grained pyroxenite showed absorption features at 460-727, 979, 1000, 1401, 1422, 1800, 1913, 1930, 2203, 2258, 2321, 2388 and 2421nm. ANOVAs and Bonferroni tests were applied to the spectral data to calculate significant spectral differences and between which pairs of rocks these significant differences occurred. Results showed that there were significant spectral differences between all the rock types of the Mambulu Complex. The variability of spectral characteristics within rock species was attributed to the difference in composition of fresh and weathered surfaces; and the significant spectral differences between rock samples can be attributed primarily to differences in mineral composition.

ACKNOWLEDGEMENTS

I would like to thank Mr. Isaac Abboy and Mr. Yerdashin Padayachee for their invaluable assistance with fieldwork.

To Mr. Naeem Agjee and Mr. Kamleshan Pillay, thank you for your input and guidance throughout this study, it is greatly appreciated.

I extend my warmest gratitude to the staff of the Department of Environmental Science, especially Mr. Edward K. Powys. Many thanks to them for all their time and assistance.

To Ms. Zaakirah Bassa and Mr. Timothy Wiggill, what a journey it has been.

To my friends and colleagues at UKZN, thank you all for your motivation and for the good times.

Finally, to my family, thank you for all the care, support and motivation.

CHAPTER ONE

1. INTRODUCTION AND PROBLEM CONTEXTUALISATION

1.1 PREAMBLE

Remote sensing is the process of measuring, analysing and interpreting radiometric data from satellite or airborne sensors. Once acquired, this data, in the form of images, are analysed by spectrally discriminating different material surfaces. This process requires ground-truthing of the area under study in order to verify that the materials analysed have been appropriately classified (Clevers and Jongschaap, 2001). Field and laboratory spectroscopy are sub-fields of remote sensing where the radiometric data of selected materials are measured individually. These measurements may either occur *in situ*, i.e. where the material occurs naturally, or in a controlled laboratory environment. Both applications require the use of a spectroradiometer which is an instrument that records electromagnetic radiation reflected off surfaces (Curtiss and Goetz, 1999). Each surface measured is displayed on a graph of wavelength versus reflectance. Depending on the surface being measured, absorptions occur at certain wavelengths. These absorptions are characteristic for a specific surface, meaning that a surface under investigation is spectrally different from other surfaces.

1.2 CONTEXTUALISATION OF PROBLEM

South Africa possesses a wealth of natural resources. Of great economic importance are its mineral and ore reserves (Kearney, 2012; Department of Mineral Resources, 2011). Identifying areas of high mineral and ore concentrations are crucial to both the longevity and economic benefit of a particular extraction site. Also, the less time taken to identify these areas can significantly reduce costs. The application of remote sensing to mineral and ore identification can greatly increase the likelihood of locating hidden mineral and ore reserves. Lithological mapping, using remote sensing, also requires remote rock identification within an image. The above-mentioned applications require field and laboratory spectroscopy as well as the creation of a spectral library (Ben-Dor, 2001; Christensen *et al*, 2000). The fundamental application of field and laboratory spectroscopy is to supplement the analysis of remotely sensed images. The creation of a spectral library would enhance this by, firstly, providing a database of signatures against which spectra in the imagery can be compared, and secondly, adding to the existing rock

and mineral signatures in other spectral libraries (Christensen *et al*, 2000). It is within this context that the spectral characteristics of the rocks forming the Mambulu Complex were investigated.

Both field and laboratory spectroscopy are extensively used in the forestry and agriculture industries (Abdel-Rahman *et al*, 2009; Milton *et al*, 2009; Kalacska *et al*, 2007; Palacios-Orueta and Ustin, 1996). Geological applications of spectroscopy are numerous and are not limited due to lack of exposure of rocks at the surface nor due to weathering processes which may alter the spectral characteristics of a rock (Younis *et al*, 1997).

A spectral library of different rock types will form a basis for future studies of this nature. These can build on this study and expand the spectral library to include other rock types or formations in KwaZulu-Natal or South Africa. Numerous such studies may result in a single database incorporating the spectral signatures of all the common rock types found in South Africa. This would, however, require a considerable amount of time in acquiring samples, and both capturing and analyzing the spectral data.

Currently, spectral databases of economically and industrially important rocks and minerals do exist (Baldridge *et al*, 2009). These are, however, independently owned by large mining corporations and private entities. A high level of confidentiality and security is associated with the data due to the competitive nature of these organisations. It is therefore proposed that this study, together with other studies of a similar nature, provide a platform to create a central spectral database with open access to academia throughout the country.

1.3 AIM AND OBJECTIVES
1.3.1 AIM OF STUDY
- To determine whether there are significant spectral differences between the rock types forming the Mambulu Complex, a mineralised igneous intrusion in the northern part of the Natal Belt, KwaZulu-Natal.

1.3.2 OBJECTIVES OF STUDY

- To capture spectral signatures of the above rock types.
- To create a spectral library using the collected data.
- To determine characteristic absorption features for each rock type.

1.4 CHAPTER SEQUENCE

Chapter One provides an overview of the use of both large and small scale hyperspectral remote sensing in mineral mapping and identification. It also gives a list of the main aim and objectives of the study. Chapter Two is a review of literature related to this investigation. It also explains the interactions of electromagnetic radiation with rock surfaces and the processes that drive these interactions. Chapter Three describes the location and physical characteristics of the study area. This chapter also provides a detailed explanation of the methods used, during the study, to achieve the stated objectives. The emphasis of Chapter Four is on the results obtained, then the analysis of these results and finally a discussion of the findings of this study. Chapter Five documents recommendations, report limitations and an overall conclusion of the investigation.

1.5 SUMMARY

Field spectrometry has been extensively used for many decades for various scientific applications. Advances in the technologies and methodologies meant that more accurate measurements can be made, inaccessible areas sampled and several new applications identified. Although there are still issues that need to be sorted out when using this technology, future advances in technology should help deal with these issues. With regard to this study, field and laboratory spectrometry is the most accurate technique for capturing the spectral signatures of rocks, considering the scale of the study. The use of a spectroradiometer together with a sound methodology was the key to meeting the aim and objectives of the study.

<div align="center">

CHAPTER TWO

2. FIELD SPECTROSCOPY AND ITS GEOLOGICAL APPLICATIONS

</div>

2.1 INTRODUCTION

All surfaces emit or reflect electromagnetic radiation. An understanding of the processes and phenomena responsible for the emitted or reflected radiation and its subsequent measurement by a sensor helps develop characteristic identification features for these surfaces. The electromagnetic spectrum has wavelength regions where the radiation from certain surfaces is specific to that region. By spectrally identifying these regions, for a specific surface, a characteristic spectral curve is measured, which can then be used for interpretation within satellite imagery.

2.2 ELECTROMAGNETIC RADIATION

2.2.1 THE ELECTROMAGNETIC SPECTRUM

Remote sensing is based on the concept of electromagnetic energy. Electromagnetic energy refers to energy that travels through space or a physical medium in the form of electromagnetic waves. These waves move at the velocity of light, and gain energy from the interactions between their electric and magnetic fields. The waves are of different forms e.g. x-rays, gamma rays, ultraviolet rays, visible light, infrared, microwaves and radio waves (Campbell, 2002).

The electromagnetic spectrum (Figure 2.1) is a continuum of energy waves of the same speed but different wavelengths and frequency. It ranges from the shorter wavelengths (including gamma and x-rays) to the longer wavelengths (including microwaves and broadcast radio waves). There are several regions of the electromagnetic spectrum that are useful for remote sensing. These may be separated into the following spectral ranges: ultraviolet (0.001 to 0.4µm), visible (0.4 to 0.7µm), near-infrared (0.7 to 3.0µm), mid-infrared (3.0 to 30µm), far-infrared (30 µm to 1mm) and microwave (1mm-1m) (Figure 2.1), and contain specific absorption areas for most surfaces (Clark, 1999). The section of the electromagnetic spectrum with wavelengths between 0.001µm and 1mm, corresponding to ultraviolet, visible and infrared portions of the spectrum are important in remote sensing and spectroscopy and is discussed further.
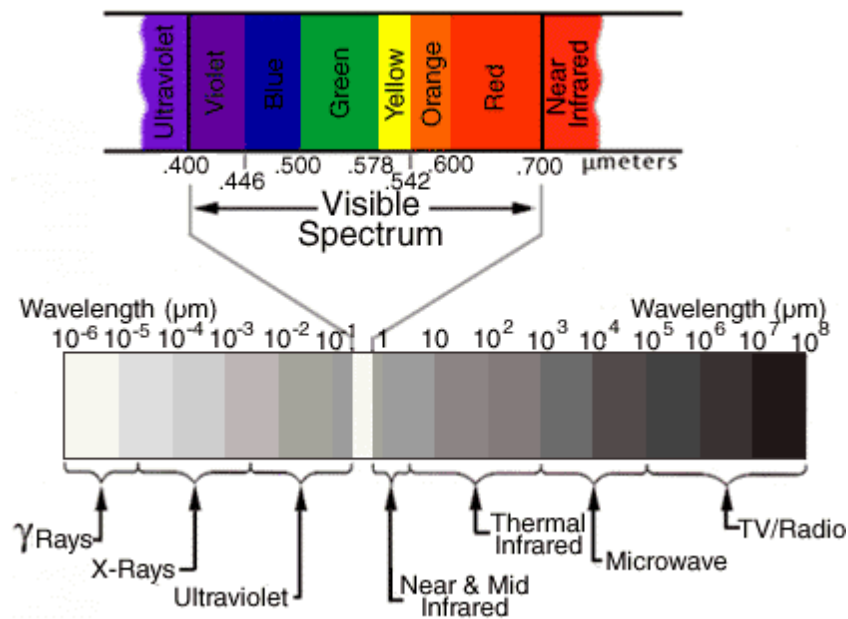
Figure 2.1 Diagram showing electromagnetic spectrum (O'Connell, 2012).

The ultraviolet (UV) portion of the electromagnetic spectrum has the shortest wavelength. The UV portion has shorter wavelengths than the visible light portion and therefore lies just beyond that portion (Figure 2.1). When materials, such as rocks and minerals, are illuminated by UV radiation, they emit or fluoresce visible light (Campbell, 2002).

The visible portion of the electromagnetic spectrum lies between 0.4 to 0.7µm (Cracknell and Hayes, 1991). The shortest wavelength of this part of the spectrum is violet and the longest wavelength is red. Visible light grades from violet through blue, green, yellow and orange to red. It is significant to remote sensing because it is this portion of the spectrum that allows humans to see colour (Campbell, 2002).

The infrared (IR) portion of the electromagnetic spectrum can be divided into the near-, mid- and far-infrared. Infrared radiation is emitted from the Earth in the form of heat. The microwave portion of the electromagnetic spectrum ranges from approximately 1mm to 100mm. This type of radiation has the longest wavelengths in terms of remote sensing (Cracknell and Hayes, 1991).

2.2.2 RADIATION

The generation of electromagnetic radiation is thought to be due to acceleration of electrical charges, changes in the energy levels of electrons, the thermal motion of atoms and molecules and the decay of radioactive substances (Bakshi and Bakshi, 2009). Since electromagnetic energy travels as waves, it is constrained by rules of wave theory. According to this theory, positive and negative electric charges produce an electric field around them. The moving charges produce a current and a current carrying conductor produces a magnetic field (Bakshi and Bakshi, 2009). The electric field moves in the same direction as the radiation, but perpendicular to it. Both the magnetic and electric fields move in the same direction, but perpendicular to each other (Campbell, 2002). Both the waves travelling in these fields travel at the speed of light (Gupta, 1991).

Electromagnetic radiation has two properties, wavelength and frequency, that are important in remote sensing (Campbell, 2002). Wavelength is the distance between consecutive wave crests or troughs. Frequency is the number of wave crests passing a certain point per unit time. Wavelength and frequency are variable whereas speed is constant. Wavelength is most commonly used to measure electromagnetic radiation in remote sensing.

2.2.2.1 INTERACTIONS WITH THE ATMOSPHERE

As electromagnetic radiation passes through the atmosphere, its intensity and spectral composition captured by a sensor may be affected. The atmosphere may cause the radiation to be scattered or absorbed (Elachi and Van Zyl, 2006).

Scattering is when gas molecules or particles in the atmosphere deflect the radiation from its original path. The amount of scattering that occurs depends on the wavelength of the radiation, abundance of gas particles, and the distance travelled by the radiation. Three types of scattering that may occur (Campbell, 2002); are Rayleigh, Mie and non-selective scattering. Rayleigh scatter is when radiation interacts with molecules smaller than the wavelength of energy. Shorter wavelengths are therefore more likely to be scattered than longer wavelengths. Mie scatter is when the diameter of the particles (such as pollen, dust, smoke and water droplets) equals the

wavelength of radiation. Non-selective scatter is when the wavelengths of the radiation are smaller than the diameter of particles (Campbell, 2002).

Absorption works in the opposite way to scattering. During this phenomenon, radiation is absorbed by molecules in the atmosphere rather than being deflected by them. The three main atmospheric molecules which absorb radiation are water vapour, carbon dioxide and ozone. Absorption plays an important role in remote sensing in that electromagnetic energy is only absorbed in certain portions of the spectrum. Atmospheric windows are portions of the spectrum wherein absorption has little or no influence on radiation (Cracknell and Hayes, 1991). Radiation with wavelengths that are not affected by absorption may therefore be used for remote sensing. The visible, thermal infrared (~10mm) and microwave (>1mm) are atmospheric windows currently being used in remote sensing (Cracknell and Hayes, 1991).

2.2.2.2 INTERACTIONS WITH SURFACES

Electromagnetic radiation that is not scattered or absorbed by atmospheric molecules may reach the Earth's surface and interact with the various surfaces that occur on it. Radiation reaching a surface may interact with that surface in one of three ways. It may be transmitted through the surface, absorbed by the surface or reflected off the surface.

Transmission occurs when radiation passes through a surface without being significantly attenuated. The transmittance of numerous materials varies greatly with wavelengths, for example, plants leaves are opaque to visible radiation but transmit considerable amounts of infrared radiation (Campbell, 2002).

In remote sensing, reflection is of importance because it is the reflected radiation that can be captured by sensors. Reflectance, according to van der Meer (2004), is the intensity of reflected radiation over the intensity of incident radiation. By that definition, according to Hatchell (1999), Reflectance (R), is a calculation, such that for a given wavelength:

R = Energy reflected from the target / Energy incident on the target

For optical radiant energy, radiance (L) is used to quantify the optical radiant energy. Radiance has the units, Watts per square metre per steradian per nanometer ($W/m^2/str/nm$). If L_t is radiance reflected from the target, and L_i is radiance incident on a target, then for a given wavelength:

$R = L_t / L_i$

This calculation of R cancels out the units ($W/m^2/str/nm$) (Hatchell, 1999). Therefore there are no units when displaying reflectance values.

Two types of reflection may occur when radiation reflects off a surface. Specular reflection is a mirror-like reflection off smooth surfaces. Almost all of the radiation is reflected in a single direction away from the surface. Diffuse reflection occurs off rough surfaces and here, radiation is reflected in several directions (Elachi and Van Zyl, 2006).

Specular and diffuse reflections are the two extremes of reflection from surfaces (van der Meer, 2001). In reality, most surfaces reflect somewhere between these two extremes. The type of reflection that may occur depends primarily on the surface roughness of a particular feature. The wavelength of incoming radiation is not as significant in determining the type of reflection. Wavelengths smaller than surface roughness or particle size would cause diffuse reflection to dominate (Elachi and Van Zyl, 2006).

The concept of bidirectional reflectance-distribution function (BRDF) will be introduced to explain the effects of diffuse reflection. BRDF is a mathematical function that relates incident irradiance from a given direction to its contribution to reflected radiance in another direction (Milton *et al*, 2009). Simply put, it is the angle that incoming solar radiation strikes a surface related to the observed reflected angle. This concept is discussed in detail in section 2.3.6.

2.2.3 SENSORS

Sensors are instruments that measure reflected electromagnetic radiation. These instruments range in size and are designed to capture specific portions of the electromagnetic spectrum.

Sensors may be categorized as passive or active, depending on the source of electromagnetic radiation.

Passive sensors capture electromagnetic radiation that is reflected naturally off surfaces meaning that radiation can only be detected if that radiation is available. With regard to reflected radiation, this is only possible when the Sun's radiation is being reflected off the Earth's surface. This is not possible at night because there is no reflected energy available from the Sun (Cracknell and Hayes, 1991). Thermal IR is naturally emitted energy (such as that of the Earth) that can be detected even at night, but levels need to be high enough to be recorded.

There are different types of passive sensors. These range from hand-held devices to complex instruments mounted on satellites. Video cameras are one of the simplest forms of passive sensors. These sensors mostly detect radiation in the visible portion of the electromagnetic spectrum, but some are designed to capture in the thermal infrared portion of the spectrum. A multispectral scanner detects radiation in both the visible and IR portions of the spectrum. Imaging spectrometers detect narrow spectral bands. Thermal scanners detect thermal signatures (8-14nm) that are directly related to the temperature of a target. Microwave radiometers detect radiation of the longer wavelengths (1-100cm). These will be discussed in the following sections.

In contrast to passive sensors, active sensors emit their own source for illumination. These sensors emit radiation directly toward the target and thereafter capture the reflected radiation. This is beneficial to remote sensing because data can be acquired day or night and in any season. Also, the illumination of targets is better controlled. The drawback of using active sensors is that they require large amounts of energy to illuminate a target. Radar and sonar are two examples of active sensors currently used in remote sensing.

Spectroradiometers are generally designed to capture specific portions of the electromagnetic spectrum by mimicking the airborne and spaceborne sensors (Asrar, 1989). All sensors, whether field-based, air- or spaceborne capture radiation and convert this data into output energy units. For air- and spaceborne sensors this output would be in the form of an image (spatial and

spectral information), with each pixel representing an energy unit; while for field-based sensors it would be represented as a spectral curve (non-spatial).

2.2.4 PLATFORMS

Sensors need to be mounted on stable platforms that are some distance from the surface or target being observed. Platforms may be categorized according to the altitude in which they travel. Spaceborne platforms occupy areas in space. These types of platforms are very large and include satellites and space stations. Airborne platforms refer to aircraft, such as airplanes, helicopters, airships, balloons or kites that have been modified to carry sensors. With regard to portable spectroradiometers, these instruments may be used by hand or mounted on yokes, lightweight masts, dedicated towers and even tramways (Milton *et al*, 2009). These pieces of equipment are usually adopted when stable platforms are required for multiple measurements or when a target is in a small, physically inaccessible area.

2.2.5 RESOLUTION

Spatial and spectral resolution are the two types relevant in remote sensing. Spatial resolution is the size of the smallest possible feature that can be detected. It depends largely on the Instantaneous Field Of View (IFOV). IFOV is the angular cone of visibility from the sensor to the target surface (van der Meer *et al*, 2001). It determines the area on the Earth's surface that is being observed from a particular altitude at any point in time (resolution cell). Scale also plays an important role in spatial resolution. Coarse or low resolution images cover a larger per pixel area where only large features and objects are visible. Fine or high resolution images cover very small per pixel areas but here, small and more detailed objects and features are visible (van der Meer *et al*, 2001). With regard to spectroscopy, spatial resolution is determined by the lens size and distance from the target. Optical lenses for spectroradiometers range from contact probes to larger degree lenses. These also depend on the type of radiometer and the application for which it is being used. A larger lens, for example, covers a greater area and would therefore be used in large-scale applications such as *in situ* soil or canopy measurements, while the smaller lenses, such as the 1° or contact probes are used for leaf or rock sample measurements (van der Meer *et al*, 2001).

Spectral resolution refers to the ability of a sensor to detect fine wavelengths. Sensors with fine resolution detect narrower wavelength ranges for a specific band or channel. Panchromatic sensors images detect large portions of the electromagnetic spectrum per band. Black and white photography, for example, captures images in the visible portion of the spectrum only. Multispectral sensors capture images using a few bands covering just a portion of the electromagnetic spectrum. Here, bands of data are more discreet than with panchromatic data. Although this is good for distinguishing surfaces, the amount of spectral data within these images are insufficient for distinguishing different rock and mineral types (Schaepman *et al*, 2009). Hyperspectral images contain tens to hundreds of continuous bands covering a larger portion of the electromagnetic spectrum. The amount of spectral data within these images are significantly greater than those of multispectral images. Since surfaces reflect radiation at different wavelengths, it is possible to determine subtle differences between even closely related surfaces (Herold *et al*, 2004). Spectroradiometers are, in essence, portable hyperspectral sensors that capture specific target reflectance as opposed to a much larger scale image scene.

2.3 FIELD SPECTROSCOPY

Field spectroscopy is the scientific branch of physics dealing with the production, transmission, measurement and interpretation of electromagnetic radiation (Malenovsky *et al*, 2007) or simply as the quantitative measurement of radiation fluxes in the field (Meroni and Colombo, 2009). The amount of reflected radiation from a specific surface is unique to that surface. The ability to capture and measure this radiation provides a means of recording the spectral characterization of specific surfaces. Portable (hand-held) spectroradiometers are the field instruments used to capture radiation reflectance off surfaces. These are generally placed/held very close to the target when measuring, as opposed to conventional remote sensing, where the sensor and target are separated by a considerable distance.

2.3.1 PURPOSE OF FIELD SPECTROSCOPY

Field spectroscopy measurements serve three main purposes. Firstly, they are used as ground truth, verification calibration or interpretation data for most airborne or satellite remote sensing investigations (Campbell, 2002; Deering, 1989). Secondly, the data may be used to model the behaviour and relationships between electromagnetic radiation and specific surfaces or

phenomena (Campbell, 2002; Deering, 1989). Thirdly, field and laboratory data may be used to evaluate the potential of using various spectral bands for specific tasks (Deering, 1989) such as in this study, where specific absorption features determined for the rocks of the Mambulu Complex, may be used to determine which bands would be suitable for identification within imagery. This will be discussed further at a later stage (Section 4.4).

2.3.2 HISTORY AND PROGRESS OF FIELD SPECTROSCOPY

Field spectroscopy is a sub-field of remote sensing where hand-held sensors are used to capture radiation directly off natural surfaces. Field spectroscopy technology pre-dates that of imaging spectrometry and both have since been used to complement each other (Milton *et al*, 2009). According to Milton *et al* (2009), field spectroradiometers were first used to study human colour vision and the colour of the Earth's surface from the air. Numerous advances in technology led to the development, in the 1970s, of sensors capable of measuring radiation in the short-wave infrared portion of the electromagnetic spectrum, which had, at the time, just been identified as an important part of the spectrum for geological applications (Milton *et al*, 2009).

Remote sensing and its numerous sub-fields are based on the concept that surfaces reflect incoming solar radiation. The type and texture of a surface determines the strength of the reflected radiation. By capturing this radiation and converting it to a digital format, an image can be analysed and deductions made. This is a very useful tool that has numerous diverse applications, e.g. in the forestry and agriculture industry for determining yield or disease identification, assessing land cover change, flood and fire damage, and mineral and vegetation mapping (Milton *et al*, 2009; Schaepman *et al*, 2009).

Numerous types of sensors exist; each designed to capture radiation within certain wavelengths of the electromagnetic spectrum. Most commonly used is a multispectral sensor. These types of scanners capture images from a few spectral bands covering just a portion of the electromagnetic spectrum. Although this is good for distinguishing surfaces, the amount of spectral data within these images are insufficient for distinguishing different rock and mineral types. Here, hyperspectral remote sensing plays an important role. These images contain tens to hundreds of continuous bands covering a larger portion of the electromagnetic spectrum. The amount of

spectral data within these images are significantly greater than those of multispectral images. Since surfaces reflect radiation at different wavelengths, it is possible to determine subtle differences between even closely related surfaces (Schaepman *et al*, 2009).

The most limiting factor, when dealing with images and surface geology, is that the area under study needs to be sufficiently exposed. Here, an exposed geological surface needs to cover a sufficiently larger area than other materials within a pixel, so that the sensor detects the radiation predominantly reflected off that exposed surface rather than the surrounding surfaces. Another limiting factor that cannot be overlooked is that sensors record only surface features. Only the upper 5000-10000nm layer of a rock surface contributes to its spectral signature (Younis *et al*, 1997).

What differentiates field spectroscopy from conventional remote sensing is that the distance between the sensor and the surface under study is greatly reduced. In field spectroscopy, this distance may be several centimetres to a few metres. Also, field spectroscopy operates at a very high scale when compared to airborne or satellite remote sensing, i.e large number of high spectral resolution. Although remote sensing may also be used in numerous field-based exercises, there are certain limitations that pose a problem to acquiring accurate measurements and will be covered in subsequent paragraphs. It is in these cases that both laboratory and field spectroscopy become important. Exposed surfaces can be accurately measured at random points and an average taken to give a better representation of that particular surface. Rocks can be distinguished from each other by their spectral signatures in the thermal emission portion of the spectrum (Rajesh, 2004). This is highly dependent on the mineral composition of the rock in that the signatures of the rocks are mixtures of the signatures of their constituent minerals, relative to their abundance. The similarity between specific types of rocks, such as granites, may allow for a composite signature to be created. This composite signature may be used as a single representative of all rocks of that class (Rajesh, 2004). A problem does, however, arise when an exposed surface is weathered. This changes the spectral characteristics of the original surface. It is therefore important to differentiate between the spectral characteristics of the weathered surface in the field and an unweathered surface of a fresh laboratory specimen.

Intensive field management campaigns during the 1970s and early 1980s contributed greatly to the development of thematic information capability and to satellite data-processing techniques. These, however, did not expand on the electromagnetic energy-to-surface interactions and processes knowledge base of the time (Deering, 1989). Most of these focused primarily on scene-classification verification, and resulted in reduced funding and budget cuts such that very little field-based research was carried out during the mid-1980s. The First ISLSCP (International Satellite Land Surface Climatology Project) Field Experiment (FIFE) field campaign of the late 1980s attempted the simultaneous acquisition of land observations, at sufficient temporal and spatial resolutions, over an area large enough to be observable by moderate resolution satellite sensors (Deering, 1989). This was seen as an opportunity to refine ground measurement techniques and methodologies that could be repeated for various other surface-based experiments.

2.3.3 APPLICATIONS OF FIELD SPECTROSCOPY

Over the past few decades, the applications of field spectroscopy have increased and expanded to very diverse studies. In conjunction, spectrometer technology has also had to evolve to overcome the challenges of these new applications. This has resulted in a wide range of applications of spectroscopy.

Spectroscopy has been used along with imaging spectrometry to discriminate and evaluating soil spectra (Lagacherie *et al*, 2008; Demattê *et al*, 2004; Palacios-Orueta and Ustin, 1996), whilst other studies focussed on identifying expansive clay soils (Chabrillat, *et al*, 2002).

It has been used to map and monitor wetland vegetation in wetlands management (Adam and Mutanga, 2009), the spectral discrimination of vegetation types in wetlands (Schmidt and Skidmore, 2003) and numerous other vegetation studies (Abdel-Rahman, 2009; Kalacska *et al*, 2007; Mutanga *et al*, 2004).

More recent applications focus on lunar and Martian remote sensing applications (Moroz *et al*, 2009). These studies assess surface composition of these planetary bodies by using analogue rocks or soils. These types of studies also focus on determining optimum absorption band

parameters for determining ore and mineral abundances; and detecting the presence of certain minerals (Bhatt *et al*, 2012; Cloutis *et al*, 2006).

2.3.4 FIELD SPECTROSCOPY IN GEOLOGY

Geological applications utilizing field spectroscopy usually occur at the data collection phase of a study. Here, spectral data are required as a reference to image data. Although this forms just a small portion of the study, the measured spectral data will determine the accuracy of the study outcome.

Since the 1930s aerial photography has played an important role in reconnaissance-level geological mapping, e.g. mapping of fractures (joints and faults), hazard assessment and rock-type discrimination (Goetz, 1989). The advent of satellite imagery in the 1960s brought about the development of more spectrally advanced data in the visible and near-infrared portion of the spectrum as well as image processing techniques that could derive spectral signatures of rock types. This process however required intensive field and laboratory studies to verify results of the image-acquired data. The mid- to late 1970s saw the development of field spectroradiometers and with it, a new respect for the understanding of the interaction between electromagnetic energy and surfaces (Goetz, 1989).

During the mid-1980s numerous studies involving the use of spectroscopy were published (see below). Even though spectroscopy was relatively new in remote sensing, at this time, the technique and the methodology of measuring spectral data have remained the same. Mehta (1985), used a spectroradiometer and spectrophotometer to study the spectral reflectance of soil-forming minerals. Minerals within the soil could be distinguished based on their percentage reflectance at certain wavelengths.

Bai-Lin and Xuan (1985) measured near-infrared reflection and infrared absorption spectra on iron deposits and related rocks from Eastern China. The focus was specifically on the spectral features of iron ores, igneous, carbonate, silicate and altered rocks. Here, measurements were taken *in-situ* and in the laboratory and were then analysed to discriminate differences.

Wester and Lunden (1985), measured the spectral reflectance of Icelandic basalts between 0.4-2.3µm using a spectroradiometer. The aim of that study was to look for differences in spectral reflectance due to the age of the basalts. Comparisons of measurements were made between weathered and cut-rock surfaces from four different Icelandic lava flows of interglacial and postglacial age. The results concluded that freshly cut surface have very similar reflectance values; while lichen-free weathered samples were spectrally featureless; and signature curves from weathered samples indicated that the older the basalt the higher the reflectance.

The renewed interest in both field spectral measurements and laboratory spectroradiometry led to the realisation that the coverage of imaging instruments eliminated the 1.6-2.5µm region that contained 'diagnostic vibrational overtone features important to geologic mapping' (Goetz, 1989: 492). The 2.0-2.5µm region, especially, contains diagnostic features for minerals containing OH^- and CO_3^- ions. During the late 1970s the importance of higher spectral resolution data in the 0.4-2.5µm region together with multispectral data from the thermal infrared region brought about the development of new airborne sensors that would greatly improve remote mineral identification. There was a concurrent development of a field spectrometer with the capability of acquiring data at more than twice the spectral resolution of the Airborne Visible Infrared Imaging Spectrometer (AVIRIS) in only 2 seconds (Goetz, 1989). Measurement of the spectral reflectance intrapixel variance was first made possible with the development of the Portable Instant Display and Analysis Spectrometer (PIDAS) (Goetz, 1989).

The past 35 years has seen a vast number of developments and improvements, in field and laboratory instruments and the techniques used for various applications. With regard to geological applications, these developments sought to improve the surface mineralogy identification process by building on the knowledge-base of energy-surface interactions (Goetz, 1989). To fulfill the requirements of this study with the use of a spectroradiometer, a better understanding of the reflectance properties of minerals is required. This will be discussed in the next subsection.

2.3.5 SPECTRAL PROPERTIES OF MINERALS

The interaction between electromagnetic energy and the geological surface being observed, or measured, is key to obtaining information from data. According to (Goetz, 1989: 493), 'the radiance measured by a sensor is related to the irradiance on a Lambert surface'. In remote sensing, this is commonly referred to as bidirectional reflectance, ρ (λ), which will be discussed in subsequent sections. Simplified, bidirectional reflectance may be represented as:

$$\rho\ (\lambda) = R_s / R_d$$

where R_s is the sample reflectance and R_d is the reflectance of a standard reference (such as Spectralon). Bidirectional reflectance is most important in the visible (0.4-0.7µm, near-infrared (0.7-1.1µm) and the short-wave infrared (1.1-2.5µm) wavelengths (Goetz, 1989). The thermal infrared region, which accounts for over 99% of the energy received by a sensor, is emitted from the Earth's surface. Here, the emittance, E (λ), is the parameter of interest.

The interaction of electromagnetic radiation with geological surfaces on a macroscopic level (e.g. diffraction, refraction and scattering) may be described by Maxwell's equations. However, on a microscopic level, when dealing with minerals, crystal lattices and their corresponding molecules play an important role, and are best described by quantum mechanics and the particulate view of electromagnetic energy (Goetz, 1989). Absorption features characteristic to each mineral are dependent on the particular crystal structure in which the absorbing species are contained and the chemical structure of the material (van der Meer, 2004).

The characteristic spectral absorption features of minerals are a combination of both scattering and absorption and are dependent on quantum mechanical interactions, particle size and single-scatter albedo (Goetz, 1989). Although energy is scattered by a surface, absorption features are created due to transmission through a particle (Goetz, 1989). Van der Meer (2004) states that variables characterizing absorption features are directly related to the structure and chemistry of the sample. Also, the absorption-band depth is related to the grain or particle-size. This is because the amount of light absorbed and scattered by a grain is dependent on grain size (van der Meer, 2004).

Electronic and vibrational interactions are the two most important types of interactions between photons and crystal lattices. These interactions cause the diagnostic absorption features in reflectance spectra in the 0.4-14µm optical region. Electronic transitions are the 'changes in the energy state of electrons bound to atoms or molecules or lattices' (Goetz, 1989: 494). This type of interaction creates diagnostic absorption features at wavelengths less than 2µm. These electronic transitions require higher energy levels and therefore occur at shorter wavelengths (Goetz, 1989). Vibrational processes relate to the vibrations of molecules in lattices and result in small displacements of the atoms. The instruments and techniques used to detect these displacements fall within a different sub-discipline of chemistry and geology and will therefore not be discussed.

According to Cloutis et al (2010), a number of absorption features that are indicative of petrogenic conditions are exhibited by pyroxene reflectance spectra. Included in these are major absorption bands at 1000- and 2000nm due to spin-allowed Fe^{2+} crystal field transitions, and numerous minor absorption bands, attributed to spin-forbidden transitions and intervalence charge transfers involving Fe^{2+} and other transition series elements, at shorter wavelengths. The presence of Fe^{2+} in both clinopyroxenes (high-calcium pyroxenes) and orthopyroxenes (low-calcium pyroxenes) leads to two spin-allowed crystal field transition absorption bands near 900nm and 1200nm for Fe^{2+} in M1 sites, and near 1000nm and 2000nm for Fe^{2+} in M2 sites (Cloutis et al, 2010). Additional weaker and narrower absorption bands are exhibited at shorter wavelengths, the most prominent of these appearing near 425, 445, 480, 505 and 545nm, all of which are attributed to spin-forbidden crystal field transitions in Fe^{2+} located in the M2 site. A 506nm absorption feature is the most intense of the shorter wavelength bands, and was nearly ubiquitous in low-calcium pyroxenes for both powders and whole rocks in a study conducted by Cloutis et al (2010).

2.3.6 BRDF

Bidirectional Reflectance Distribution Function (BRDF) is an intrinsic physical property that governs the reflectance characteristics of a surface (Campbell, 2002; Deering, 1989). It is a mathematical concept describing reflectance behaviour with regard to angles of illumination and

observation. Here, the concept of a Lambertian surface is used to approximate the reflectance behaviour of surfaces. BRDF for a true Lambertian surface has perfectly diffuse reflection. This is, however, only true for Lambertian surfaces which are usually represented by an ideal, standard reference surface. Natural surfaces, on the other hand, exhibit non-Lambertian or more complex reflectance behaviour depending on surface geometry (Campbell, 2002; Deering, 1989).
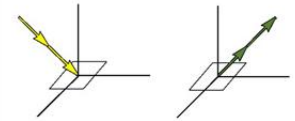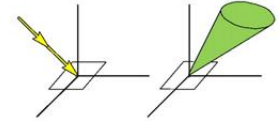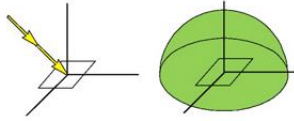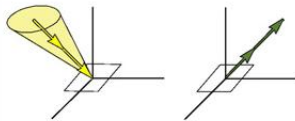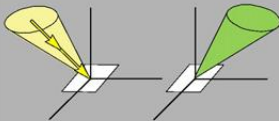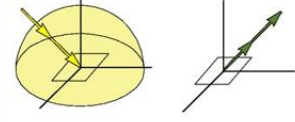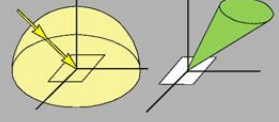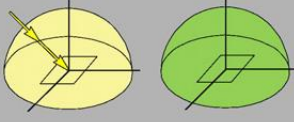
Incoming/Reflected	Directional	Conical	Hemispherical
Directional	Bidirectional Case 1	Directional-conical Case 2	Directional-hemispherical Case 3
Conical	Conical-directional Case 4	Biconical Case 5	Conical-hemispherical Case 6
Hemispherical	Hemispherical-directional Case 7	Hemispherical-conical Case 8	Bihemispherical Case 9

Figure 2.2 Terminology used to describe relationship between incoming and reflected radiance quantities (after Milton *et al*, 2009).

Milton *et al* (2009), based a different classification system on work by Nicodemus *et al* (1977) and Schaepman-Strub et al (2006), where the classification represents the relation of incoming and reflected radiance to describe reflectance quantities (Figure 2.2). From this, it was proposed that the nature of the incident or reflected radiation could be directional, conical or hemispherical. This type of classification brought about nine different combinations to describe reflectance measurements. However, applying this classification to real-world field situations posed problems.

2.4 PHYSICAL, CHEMICAL AND REFLECTANCE PROPERTIES OF ROCKS FROM THE MAMBULU COMPLEX

2.4.1 MASSIF-TYPE ANORTHOSITE

Anorthosite is a plutonic igneous rock in which at least 90% of the total feldspar is plagioclase (Plate 2.1) (Ashwal 1993; Middlemost, 1985; Barker, 1983 MacKenzie *et al*, 1982). The various types of anorthosites that exist depend on the type of occurrence and the composition of plagioclase. The plagioclase in anorthosite generally comprises more than 30% anorthite (Barker, 1983). Also present are small amounts of the Fe/Mg minerals pyroxene (Le Maitre, 2004) olivine and other opaque minerals (Anbazhagan and Arivazhagan, 2010). Much work has been done on the various types of anorthosite covering its diverse spatial and temporal extent. Focus, here, will be on Proterozoic, or massif-type, anorthosite as it is this type that is found in the study area.
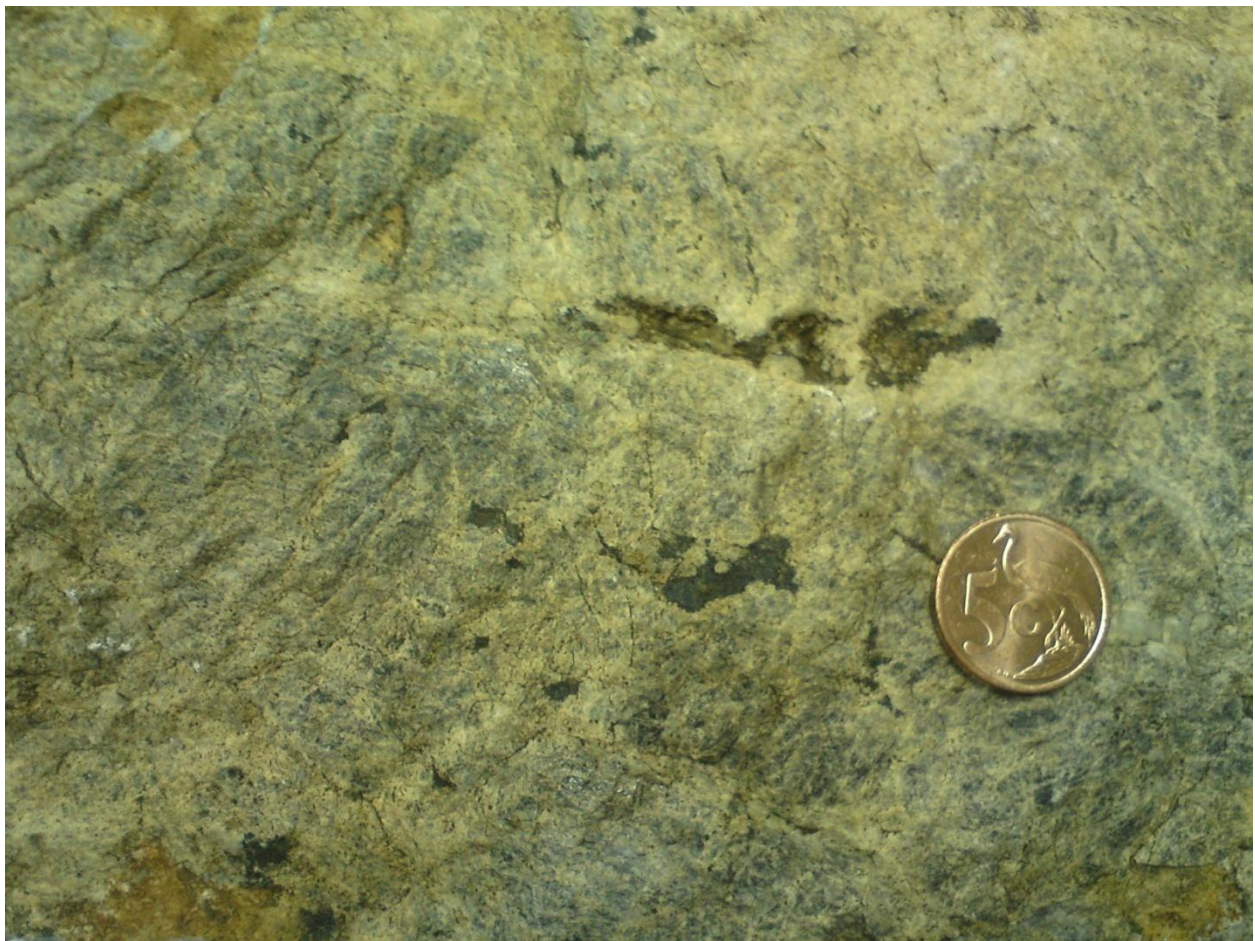
Plate 2.1 Weathered surface of anorthosite from the Mambulu Complex. Coin shown for scale, diameter of 20mm (photograph by I. Mustapha).

Proterozoic massif-type anorthosites are large plutonic masses, essentially non-stratiform domical structures (Middlemost, 1985); and typically cover areas exceeding 10 000km^2. Massif-type anorthosite comprises the most voluminous anorthosite type on Earth (Ashwal, 1993). This may be the result of the emplacement of two extensive belts of igneous rocks in both Gondwanaland and Laurasia (Middlemost, 1985). The southern belt (within which lies the Mambulu Complex) has not been as widely studied as its larger northern counterpart.

2.4.2 LEUCO-GABBRO

Gabbros are medium- to coarse-grained, dark- to medium-coloured intrusive rocks (Plate 2.2) (Middlemost, 1985; MacKenzie *et al*, 1982) and geologically are the plutonic (intruded at depth) equivalent of dolerite and basalt. Chemical and modal compositions of these rocks vary greatly, but comprise primarily of augite (pyroxene) and a plagioclase of labradorite, or a more calcic composition (MacKenzie *et al*, 1982). Extreme variation in composition can result in gabbro grading into pyroxenite or even peridotite (significant increase in percentage volume of pyroxene), while leuco-gabbro grades into anorthosite (Middlemost, 1985; MacKenzie *et al*, 1982). Apart from occurring as sills, dykes and plugs, voluminous amounts of gabbros are found as major units within the great layered intrusions, e.g. Bushveld Complex of South Africa. The gabbro at Mambulu is referred to as leuco-gabbro (McCourt *et al*, 2006) because it comprises 'considerably more felsic minerals than would be regarded as normal for that rock type' (Le Maitre, 2004: 103). This should, in theory, make leuco-gabbro spectrally distinct from gabbro. Leuco-gabbro comprises the minerals plagioclase feldspar (87.8%), clinopyroxene (3.1%), olivine (7%), biotite (0.6%), opaques (1%) and 0.5% accessory minerals (Bowden *et al*, (1987).

Reflectance spectra of gabbro measures by Qaid *et al* (2009) showed intense absorption features in the 1.4, 1.9, 2.34, and 2.4µm regions representing OH, H_2O and CO_3^{-2} respectively. There is also a ferrous absorption at 0.9µm. Two hydroxyl bonds centred around 2.26µm and 2.32µm also characterise gabbro spectra (Qaid *et al*, 2009).

Plate 2.2 Weathered surface of coarse-grained leuco-gabbro from the Mambulu Complex. Coin shown for scale, diameter of 20mm (photograph by I. Mustapha).

2.4.3 MAGNETITITE

The mineral magnetite (the iron ferrite $Fe(Fe_2O_4)$) forms from the dehydration of $Fe(OH)^2$ and requires intermediate Eh and high pH (Belikov *et al*, 2002; Lewis and McConchie, 1994). It has an octahedral structure that is both a characteristic feature and a diagnostic sign of the compound (Belikov *et al*, 2002). According to Lewis and McConchie (1994), it is referred to as titanomagnetite when in solid solution with ulvospinel. Plate 2.3 shows a sample of magnetitite from the Mambulu Complex. Magnetite absorption is observed at 370-380cm^{-1} (Belikov *et al*, 2002), and centred around 570cm^{-1} (Belikov *et al*, 2002; Liese, 1967).

Plate 2.3 Weathered surface of magnetitite from the Mambulu Complex. Coin shown for scale, diameter of 22mm (photograph by I. Mustapha).

2.4.4 PYROXENITE

Pyroxenite is an ultramafic rock predominantly consisting of one or more of the pyroxene group of minerals with accessory minerals such as olivine, garnet, spinel, biotite, hornblende, plagioclase feldspar and nepheline (Plate 2.4) (Le Maitre, 2004; MacKenzie, *et al*, 1982). Numerous major absorption features of pyroxene occur between the 1000 and 2000nm regions with minor absorption features at shorter (425, 445, 480, 505 and 545nm) wavelengths (Cloutis *et al*, 2010). The most defined of these shorter wavelengths is the 506nm absorption feature characteristic of (low-calcium) orthopyroxene (Cloutis *et al*, 2010).

Plate 2.4 Weathered surface of medium-grained pyroxenite from the Mambulu Complex. Coin shown for scale, diameter of 22mm (photograph by I. Mustapha).

Spectra of pyroxenite rocks determined by Qaid *et al* (2009) showed well defined absorption features at 0.7μm and 1.0μm, which corresponded to the ferric and ferrous ions. Also present was an absorption feature at 2.26μm due to the presence of Fe-OH, and two more intense absorptions at 2.32μm and 2.39μm due to the presence of Fe.Mg-OH bonds (Qaid *et al*, 2009).

2.5 CONCLUSION

The interactions of electromagnetic radiation with various surfaces influence the mechanical and spectral properties of the resultant reflected radiation. It is these altered spectral properties that give rise to diagnostic absorption features for different surfaces. The technology and techniques of spectroscopy have come a long way over the last 45 years. Present applications are found in almost all the natural sciences and incorporate theory from the physical, chemical and

mathematical sciences. With regard to the present study, the physical and chemical properties of the rocks of the Mambulu Complex should affect their spectral properties, and as a result give rise to absorption features, at specific wavelengths, that are diagnostic for each rock type.

CHAPTER THREE
3. STUDY AREA AND METHODOLOGY

3.1 INTRODUCTION

The area of study is situated in the northeastern part of KwaZulu-Natal, South Africa (Figure 3.1). The specific suite of rocks under study forms the Mambulu Complex, a mineralised unit in the Tugela Terrane, Natal Belt, which is in turn part of the Namaqua-Natal Metamorphic Province. The Namaqua-Natal Metamorphic Province is a geological entity formed in the Mesoproterozoic between 1250 and 1000 million years ago (McCourt *et al*, 2006 and references therein). The Namaqua portion of this belt occurs in southern Namibia and stretches southeastwards where it is exposed in KwaZulu-Natal (Natal belt). This suite of rocks was chosen because it represents material extruded from the same magmatic event, i.e. rocks that have similar composition.

Figure 3.1 Map showing the location of the study area (in red) within KwaZulu-Natal. Main towns are shown for reference. Inset map shows the position of KZN within South Africa.

3.2 STUDY AREA

3.2.1 PHYSIOGRAPHY

The topography of the area is strongly influenced by the drainage system of the Tugela River and its associated tributaries. The area lies at an altitude of 450-900m above mean sea level and has a maximum vertical relief of about 1500m (Matthews and Charlesworth, 1981). The Tugela basin covers an area of 11200 square miles and comprises eight major catchments. The Mambulu Complex is situated in the Lower Tugela catchment area which is approximately 604.7 square miles in area (Oliff, 1960). This part of the basin is characterized by very rugged and broken terrain with more undulating landforms and a wider river valley towards the coast (Oliff, 1960).

3.2.2 CLIMATE AND RAINFALL

The Tugela Basin is situated in the subtropical climate zone, and its specific climate is influenced by both this position and its topography (Oliff, 1960). Two main climatic seasons are distinguishable: a dry, low-flow winter season which lasts from April/June to October (sometimes November); and a wet, high-flow season for the remaining months (Oliff, 1960). Mean air temperatures are 16°C in July and 22°C in January, but are also prone to extremes where summer temperatures reach 35-40°C while winter temperatures can fall to several degrees below freezing point (Oliff, 1960). Generally the basin receives most of its rainfall in summer, but this does vary within each catchment due to topography. The escarpments are characterized by very high rainfalls (1905mm) while at lower altitudes, such as in sheltered valleys and depressions it can be as low as 635mm. The coastal portion of the Tugela valley receives approximately 1103mm, but the mean annual rainfall of the Lower Tugela catchment is 907mm (Oliff, 1960). Dry thorn or valley bushveld vegetation characterizes this catchment. Ngongoni veld of the Natal mist belt is predominant on the heights around Kranskop (Oliff, 1960).

3.2.3 GEOLOGICAL SETTING

The study area is situated in the Tugela Valley to the east of Kranskop. The geology around Kranskop is dominated by red sandstone and quartz arenite of the Natal Group and overlying shale of the Ecca Group. The rocks in the Tugela Valley below this sedimentary material are metamorphic in character and form part of the Natal Belt, the eastern section of the Namaqua-Natal Metamorpic Province). The Natal Belt is dominated by granitoid rocks originating from

the mantle ~1.5 Ga and is relatively juvenile compared to the more complex Namaqua Metamorphic Complex. These rocks are mainly granitoid gneisses, supracrustal gneisses and younger intrusive rocks (McCourt *et al*, 2006). The Natal belt is divided into three tectono-metamorphic terranes, referred to, from north to south, as the Tugela, Mzumbe and Margate (McCourt *et al*, 2006; Bisnath, 2000). The area of study occurs within the Tugela Terrane, which is further sub-divided into the four thrust sheets, namely the Nkomo, Madidima, Mandleni and Tugela sheets. The Mambulu Complex intrudes into the southern part of the Mandleni thrust sheet (Bisnath *et al*, 2008; McCourt *et al*, 2006). Johnston *et al* (2003), divided this thrust sheet into the Dondwana gneiss unit, the Evuleka ultramafic unit, the Mtungweni granitoid unit and the Mambulu Complex. According to Bisnath *et al* (2008), the Mandleni thrust sheet is situated structurally below the Tugela thrust sheet and overlays the Madidima thrust sheet; two igneous complexes, the ultramafic Sithilo Complex and the layered gabbroic Mambulu Complex, intrude the rocks of the Mandleni thrust sheet (Bisnath *et al*, 2008)

The Mambulu Complex (Figure 3.2) is a small suite of igneous rocks covering approximately twenty-five square kilometres (Reynolds, 1984). It is located (-28.97°S and 31.03°E) at the confluence of the Mambulu and Tugela rivers (Reynolds, 1984). Linstrom (1987) described the complex as being composed of mainly anorthosite, diallagite, websterite, leuco- and melano-gabbronorite. According to McCourt *et al* (2006) and Reynolds (1984), the Mambulu Complex is a layered intrusion of pyroxenite, gabbro-norite, leuco-gabbro and massif-type anorthosite. These rock types characterize the southern portion of the Mambulu complex while the northern section comprises stratiform layers rich in magnetitite (McCourt *et al*, 2006; Reynolds, 1984; Matthews and Charlesworth, 1981). Near the margin of the complex, fine- to medium-grained alternating lenses of pyroxenite, norite and hornblende gabbro occur; these are traversed by coarse-grained pegmatite dykes of anorthosite and diallagite (Linstrom, 1987). Also occurring throughout the whole body, but more common in the marginal zone, are thin lenses of titaniferous magnetitite (Linstrom, 1987). The central portion of the complex is less basic and is composed of medium- to fine-grained greenish grey gabbronorite. The rocks of the Mambulu Complex preserve evidence of two phases of deformation that produced folds and ductile shear zones. The rock layers dip towards the centre at between 10° and 40° (Eales *et al*, 1988). The age of the Mambulu Complex is 1145Ma (McCourt *et al*, 2006).
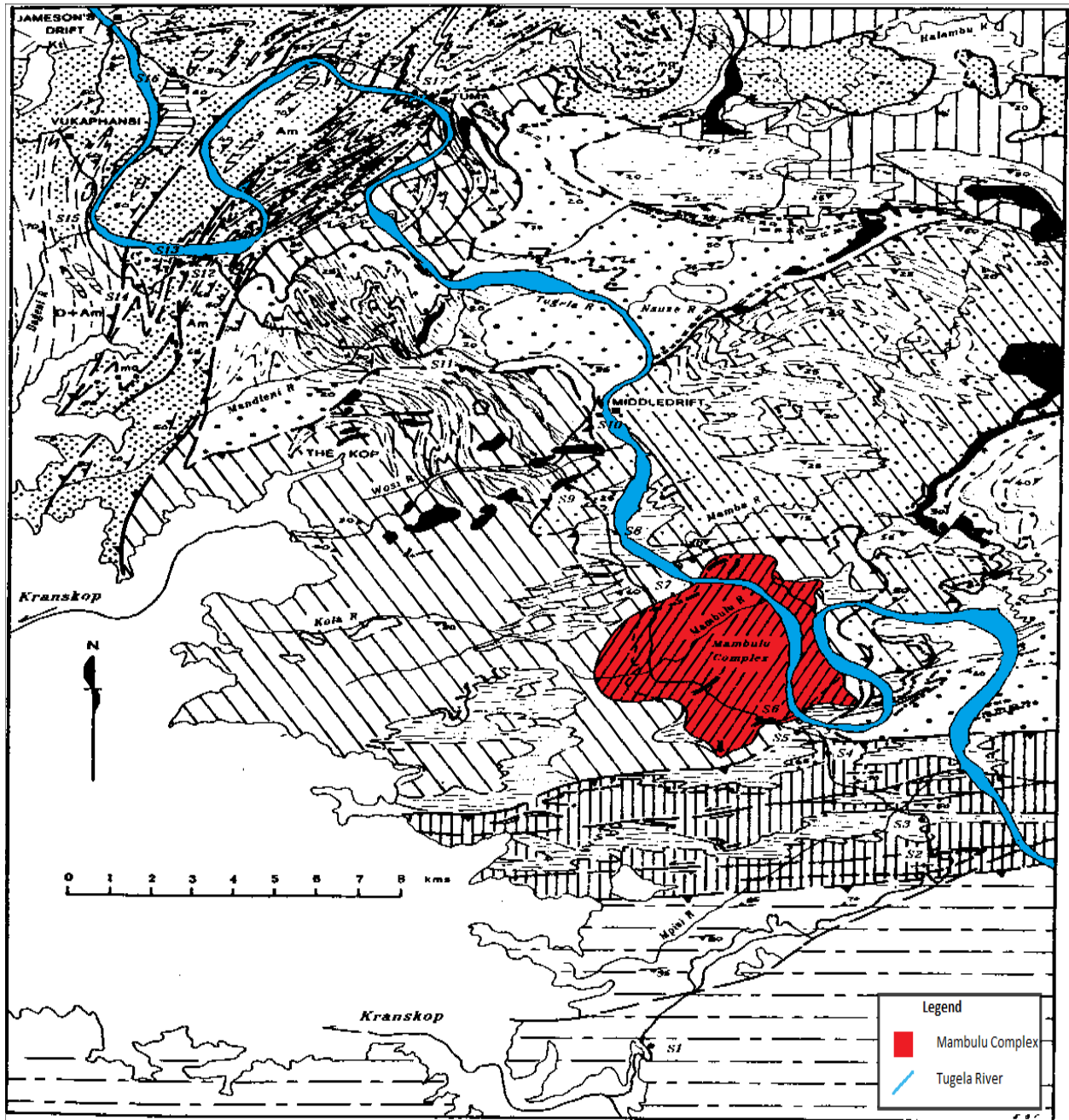
Figure 3.2 Geological map of the Mambulu Complex (in red) and surrounding geology (after Matthews and Charlesworth, 1981). Other rock types are indicated by various forms of shading

3.3 METHODOLOGY

3.3.1 ROCK SAMPLE COLLECTION

Rock samples (viz. anorthosite, leuco-gabbro, magnetitite and pyroxenite) were collected using a purposive sampling technique. According to Debba *et al* (2005), this is a common geological

sampling method where observations are made in linear traverses and the skills and knowledge of a skilled field worker becomes important. There is a two-fold purpose to acquiring the samples; spectral signatures have to be captured both in the field and in the laboratory, which would in effect mimic natural and controlled conditions respectively. However, this study focussed on the spectral signatures captured under laboratory conditions. Samples were acquired along a north-south traverse along the western bank of the Tugela River (Figure 3.2). Here, rock outcrops of the Mambulu Complex are excellent and easily accessible. Only samples of anorthosite, leuco-gabbro, magnetitite and pyroxenite were exposed and visible along the traverse. These four rock types were therefore chosen for this study. Rock samples of both fresh and weathered surfaces were broken off parent rock using a sledge hammer and then trimmed using a standard geological hammer. The samples were stored in marked plastic bags and taken back to the laboratory for spectral measurements.

3.3.2 EXPERIMENTAL DESIGN AND ROCK SPECTRAL MEASUREMENTS

Field spectroradiometers are hand-held sensing devices, used to accurately capture radiation reflected from a surface or the specific spectral signature of a surface. These instruments are highly sensitive to differences in radiation and light. In order to optimize measurements, Milton *et al* (2009) recommend a method whereby the sensor head is mounted on a pole or yoke, positioned some distance away from the operator's body. In effect, this will minimize the amount of scattered light from clothing falling onto surfaces.

The ASD Fieldspec 3 spectroradiometer is a spectroradiometer that measures spectra between 400 and 2500nm, and has a bandwidth of 1nm (Zeng, *et al*, 2003). RS_3™ software interfaces with and enables the Fieldspec instrument to measure spectral data. The spectroradiometer was set up in a laboratory dark room in the Department of Environmental Science at UKZN. The ambient temperature was fixed at 17°C as this was found to be the optimal temperature to correct humidity effects. A 50W halogen lamp, which was the only source of illumination, was positioned nadir to the sampling surface. All measurements were carried out inside a confined 'black box' (a cardboard box painted black using matte paint) to eliminate the effects of reflection from clothing and background reflection. Once the instrument was calibrated, using a Spectralon white reference panel, spectral readings were taken of the rock samples. The fibre

optic cable (1° field of view) was fixed in nadir position at 0.4m above the sample. This gave a Ground Field of View of 9.3cm. For each sample, three readings per rotation of 120° were captured, giving a total of nine readings per sample. This was done to cancel out the effects of bias as natural rock surfaces are uneven and readings would vary depending on the angle of illumination. The process was done for both fresh and weathered surfaces.

The ViewSpec Pro version 6.0.11 (ASD, 2008) spectral post-processing software was used to analyze the spectral data. All reflectance measurements were first imported to ASCII and then converted to MS Excel format to enable statistical analysis using the Statistical Package for the Social Sciences (SPSS, 2010).

3.3.3 SPECTRAL TRANSFORMATION

Continuum removal is a process whereby reflectance spectra are normalized to allow comparison of individual absorption features from a common baseline (Gomez *et al*, 2008; Mutanga *et al*, 2004). The aim of continuum removal is to quantify the absorption of materials at a specific wavelength and is based on the assumption that no other material has strong absorption at the selected wavelength (Gomez *et al*, 2008). A convex hull is applied to that part of the spectrum to be analysed (Noomen *et al*, 2006). The resulting curve has values from 0 to 1, emphasizing the position and depth of the absorption feature (Schmidt and Skidmore, 2003). Here, the actual values are not important; rather this technique performs a vertical stretch of the entire curve, which enhances the depth of absorption features. Continuum removal for spectra measured for the Mambulu samples was done using the ENVI version 4.7 (ENVI, 2009) remote sensing software.

3.3.4 COMPARATIVE ANALYSIS OF REFLECTANCE SPECTRA

All statistical analyses were performed in the SPSS (by IBM) statistics package. Analysis of Variance (ANOVAs) was applied to those bands with distinct absorption features, to determine significant differences within a sample. These were applied to every wavelength in each absorption feature, for all samples. The main purpose of using ANOVAs was to establish whether significant differences between rocks occurred at the wavelength of interest.

The Bonferroni test is a multi-comparisons test, which was applied to the absorption wavelengths across all the samples of all rock types, to show where differences lie. At each wavelength of interest, the Bonferroni test compared one sample against each of the other Mambulu samples in a pairwise manner. The significance for each pair is calculated and returned as a value between 0 and 1. If this value is less than 0.05 then the samples in that particular pair are significantly different from each other.

Since absorption regions may be characteristic for each rock type, it is possible to determine whether statistically significant differences occur in these absorption regions. Statistical analysis was done by running ANOVAs on all wavelengths in the absorption regions. Thereafter, Bonferroni tests were applied to these wavelengths to determine where (comparison between pairs of rocks for all combinations) these significant differences occurred. Here, for each absorption wavelength, for each rock type, comparisons were made against the other remaining rock types to determine which rock type was significantly different from the target rock, e.g. anorthosite, at a particular wavelength, would be significantly different from other rocks, based on their ANOVA values. Also, fresh and weathered samples at each wavelength were analysed and treated as individual samples, due to them having different spectral properties.

3.4 CONCLUSION

The spectral reflectances of rocks from the Mambulu Complex were measured using a spectroradiometer. These reflectance measurements were used to identify absorption features for each sample. ANOVAs and Bonferroni tests were applied to each absorption feature to determine whether significant differences occurred between the samples, and also between which pairs these differences occurred.

CHAPTER FOUR
4. RESULTS AND DISCUSSION

4.1 INTRODUCTION

This chapter presents the results of the spectral and statistical analyses. These are thereafter discussed in detail. Spectral analysis determined the absorption band for each rock type using the continuum removal method. Continuum removal was applied to the average spectrum of each rock type. Statistical analyses comprised discrimination of these absorption bands from each other.

4.2 RESULTS

4.2.1 SPECTRAL ANALYSIS

The ENVI (version 4.7) remote sensing software by ITT Corporation, together with the ViewSpec Pro (version 6.0.11) spectral analysis software by ASD Inc. were used to visually determine characteristic absorption features for each rock type. Here, the continuum removal method was applied to each of the spectra, in order to enhance all absorptions. In this study, these absorptions were referred to as absorption 'feature' for broad- or multiple-absorption centred-features; or as an absorption 'wavelength' if a single wavelength was visibly distinguishable as the centre of that feature. The latter was only used for absorptions that had deep and narrow shapes, with a distinct single-wavelength apex as its centre. Where possible, absorption wavelengths for both fresh and weathered samples are discussed individually. In the text that follows, the numbers in brackets (e.g. 0.89) represent the reflectance at which the absorptions occurred.

For 9 measurements per each sample, the spectra were averaged and considered as representative of rock modal composition (Sgavetti *et al*, 2006). Spectral properties of rocks are affected by parameters such as mineral structure and chemistry, rock texture and grain size (Sgavetti *et al*, 2006). Variation in any of these parameters can produce both systematic and non-systematic rock spectral variability.

Diagnostic absorption features in rock and mineral spectra are a result of energy-matter interactions within molecular groups. Igneous rocks, as defined by Sgavetti et al (2006), are complex chemical systems that are constrained by specific physic-chemical conditions that affect composition, degree of crystallinity, crystal structure and texture. Rock geochemistry and petrology arising from different geologic processes affect the spectral signature of a rock. Spectral variability is therefore intrinsic to the rock-forming process, which means that 'genetically related rocks can display systematic variations of spectral parameters as functions of systematic variations of petrographical and geochemical parameters' (Sgavetti *et al*, 2006: 144). This means that there should be significant spectral differences between all the rock types used in this study. Diagnostic absorption features for each rock type were determined using the continuum removal method.

4.2.2 ANORTHOSITE

Reflectance values for fresh anorthosite were between 0.24-0.34. Spectra for fresh anorthosite displayed a gently decreasing slope (Figure 4.1). Spectra for weathered anorthosite, however, rose in the visible portion and then started to even out and follow the spectra of fresh anorthosite. For weathered anorthosite, reflectance values ranged from 0.08 to ~0.28. Most of the absorption features for both fresh and weathered samples were within 0.23 to ~0.3 reflectance range.
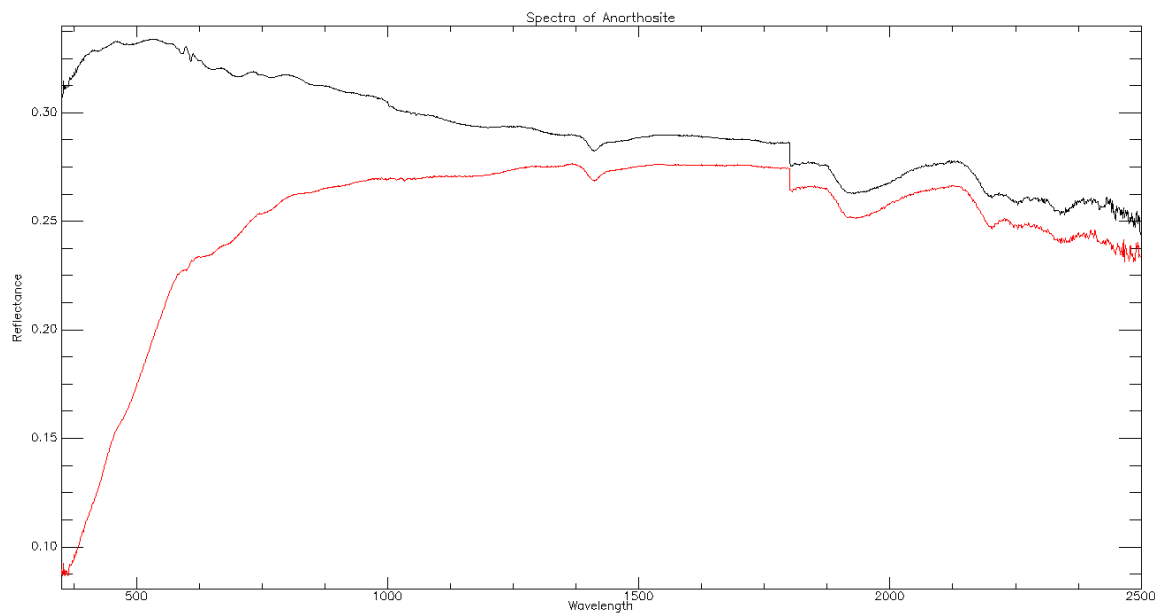
Figure 4.1 Spectral curves of fresh (black) and weathered (red) anorthosite.

Continuum-removed spectra for anorthosite (Figure 4.2) showed absorption features at 480-490, 592, 603, 608, 627-726, 765, 1410, 1905-1955, 2200, 2250 and 2330nm.

There is a very strong double-absorption feature at 480-490nm for weathered anorthosite, but this is weak for fresh samples. The centres for this absorption feature are very distinct in the spectral curve of weathered anorthosite and occur at 483nm and 489nm at a reflectance of 0.99 for fresh samples and 0.97 for weathered samples.

There were three minor absorptions at 592 (reflectance of 0.98 for fresh and 0.99 for weathered), 603 (reflectance of 0.97 for fresh and 0.99 for weathered) and 608nm reflectance of 0.97 for fresh and 0.99 for weathered). All were narrow features and were more pronounced for fresh samples. Also, these absorptions for spectra of fresh samples occurred at a lower reflectance than for spectra of weathered samples.
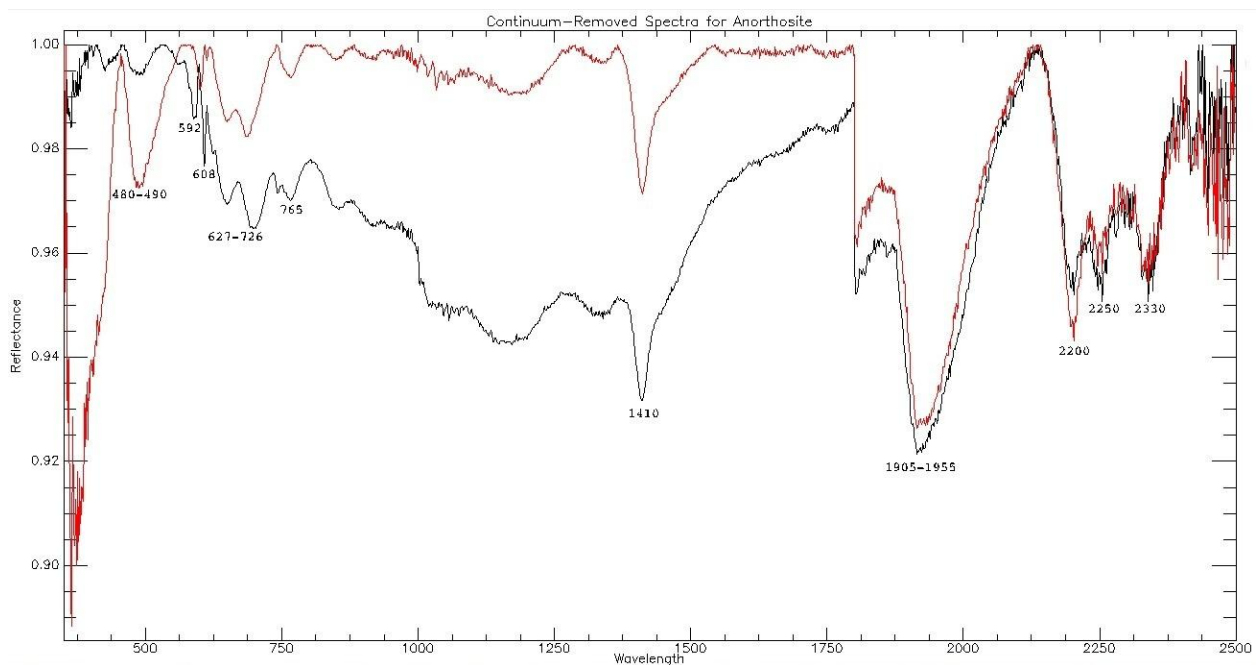
Figure 4.2 Continuum-removed spectra for fresh (black) and weathered (red) anorthosite.

A double-absorption feature was present at 627-726nm. The centres for this feature were at 648nm (at 0.96 for fresh and 0.98 for weathered), 684nm (weathered at 0.98 reflectance), and 699nm (fresh at 0.96 reflectance). Fresh samples had a lower reflectance than weathered spectra.

There was also a minor absorption at 765nm. Both fresh and weathered spectra had similar shapes, but the weathered feature was at a higher reflectance (0.99) than the fresh one (0.96).

In both fresh and weathered samples, there is a major absorption at 1410nm. This was a very narrow and deep feature for both fresh and weathered samples. The spectra for weathered samples occurred at a higher reflectance (0.97) than fresh spectra (0.93).

There was a major absorption at 1905-1955nm. The centres for this feature were at 1914nm (0.926 reflectance) for weathered samples, and at 1915nm (0.921 reflectance) for fresh samples.

The 2200nm feature was a very narrow absorption feature prevalent in both fresh and weathered samples. Weathered anorthosite showed a deeper absorption (0.945) at this wavelength.

At 2250nm, the absorption feature for fresh samples is the same (occupies the same reflectance range, 0.951) as that of the 2200nm feature. It is also a deeper absorption than for weathered anorthosite (0.958) at this wavelength.

The 2330nm absorption feature is similar to the 2250nm feature in that they both occupy a similar reflectance range. Fresh samples in these features have a slightly deeper absorption (0.952) than respective weathered samples (0.957) at those wavelengths.

4.2.3 LEUCO-GABBRO

Spectra for leuco-gabbro covered a reflectance range similar to that of anorthosite (0.12 to ~0.34). For fresh samples, spectra were very gentle, with reflectance values ranging from 0.12 to ~0.2. For weathered samples, reflectance ranged from 0.04 to ~0.34. The absorption features for both fresh and weathered samples showed almost identical absorption features across the spectrum (Figure 4.3).
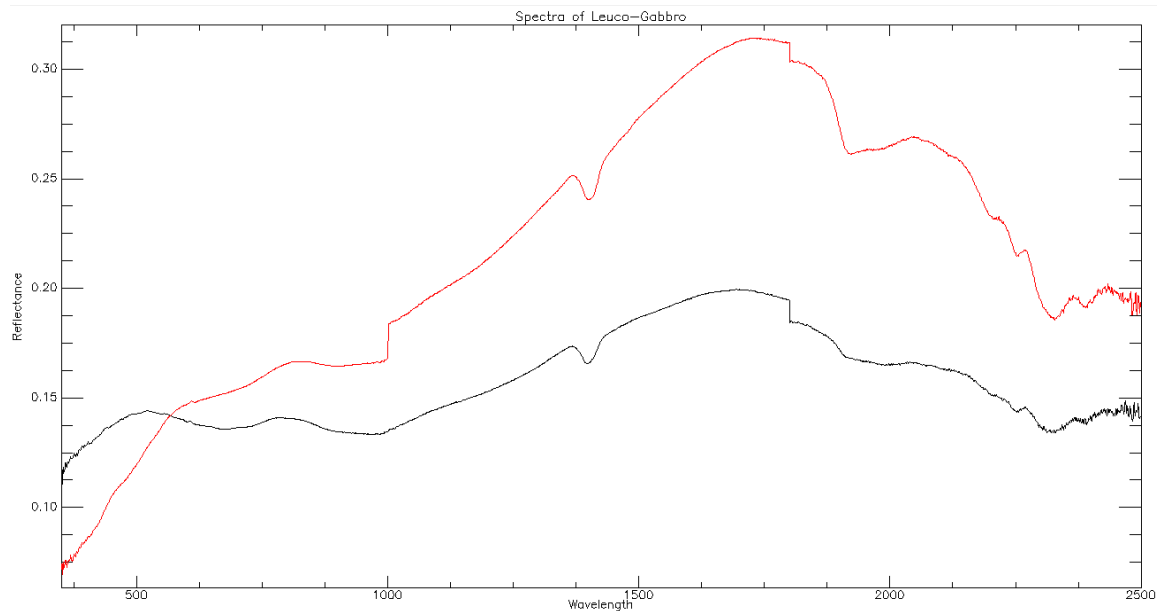
Figure 4.3 Spectral curves of fresh (black) and weathered (red) leuco-gabbro.

Leuco-gabbro is not a commonly-occurring rock and as such, has not been studied in terms of its spectral characteristics; therefore, the Mambulu spectra were compared to gabbro. For leuco-gabbro, continuum-removed spectra had absorption features at 481, 950-1010, 1407, 1917, 2206, 2252, and 2300-2340nm (Figure 4.4)

A minor absorption feature occurred at 481nm. This feature was distinct in weathered samples (0.98 reflectance) but very minor in fresh samples (0.99 reflectance).

There was a very strong absorption feature at 950-1010nm. This absorption feature has its centres at 992nm and 995nm (both at 0.8).

At 1407nm the absorption feature was very narrow and deep for both fresh and weathered samples. It sits on a strongly positive slope, from 1000nm to 1800nm at 0.89 reflectance (Figure 4.4).
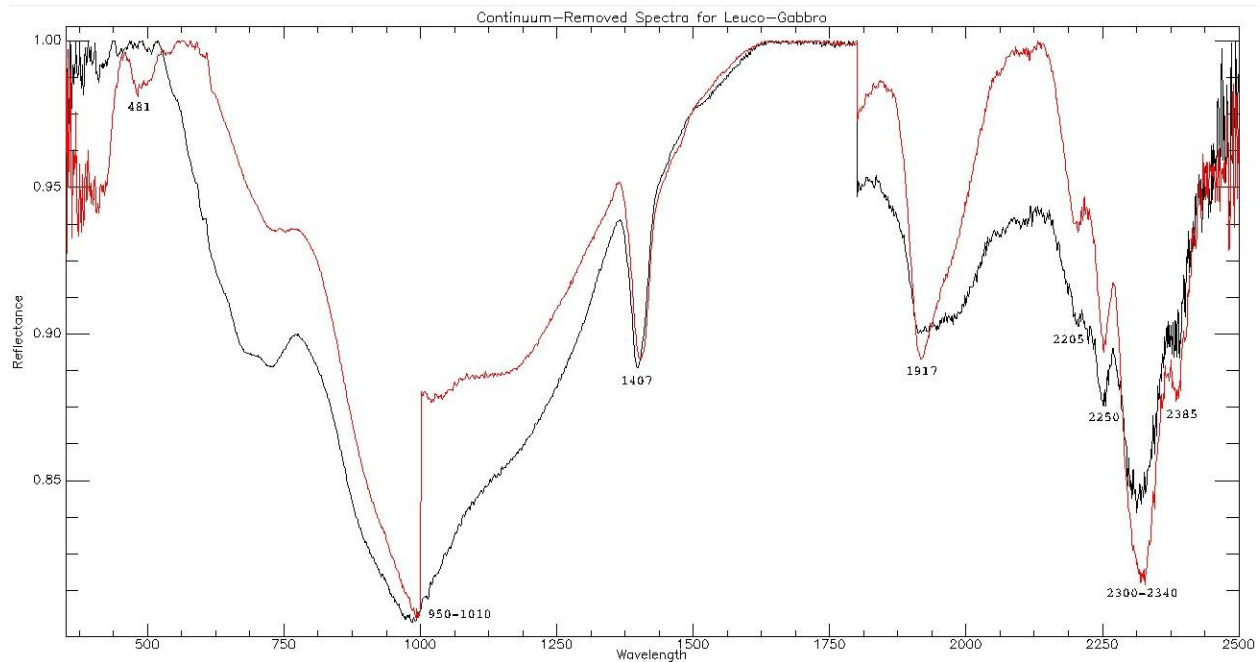
Figure 4.4 Continuum-removed spectra for fresh (black) and weathered (red) leuco-gabbro.

The 1917nm absorption feature was very broad for fresh samples, but narrow and very distinct for weathered samples. This feature was very deep for weathered samples, occupying a large reflectance range (0.89-0.97) when compared to that of fresh samples (0.90-0.92).

The absorption feature at 2205nm was a minor absorption that was more prevalent in weathered samples. Also, this feature was at a higher reflectance for weathered samples (0.93) than for fresh samples (0.90).

This was followed by the 2250nm absorption feature. Both were distinct features with weathered samples present at a higher reflectance (0.89) than fresh samples (0.87).

There was a very broad and strong absorption feature at 2300-2340nm. The absorption centres were at 2312nm for fresh samples (reflectance of 0.84) and 2321nm and 2328nm for weathered samples (reflectance of 0.81).

At 2385nm there was a minor absorption feature. Although present in both fresh and weathered samples, this absorption feature was more distinct in weathered samples. It was also symmetrically related to the 2250nm feature, in that they both flank the 2330nm major absorption feature (at 0.87 for weathered samples and 0.89 for fresh samples).

4.2.4 MAGNETITITE

Spectra for magnetitite (Figure 4.5) displayed varying shapes ranging from 0.01 to ~0.18. Although these spectra were highly variable in shape, they still had lower reflectance values and covered a smaller reflectance range than anorthosite and leuco-gabbro. Fresh samples displayed very gentle curves with reflectance values ranging from 0.08 to ~0.14. Weathered and highly weathered samples were more spectrally variable. These spectra were more undulating, than the spectra for fresh samples, and covered a higher reflectance range. Reflectance values ranged from 0.02 to ~0.13 (weathered) and 0.01 to ~0.18 (highly weathered). Also, absorption features were more distinct for weathered and highly weathered samples than for fresh samples.
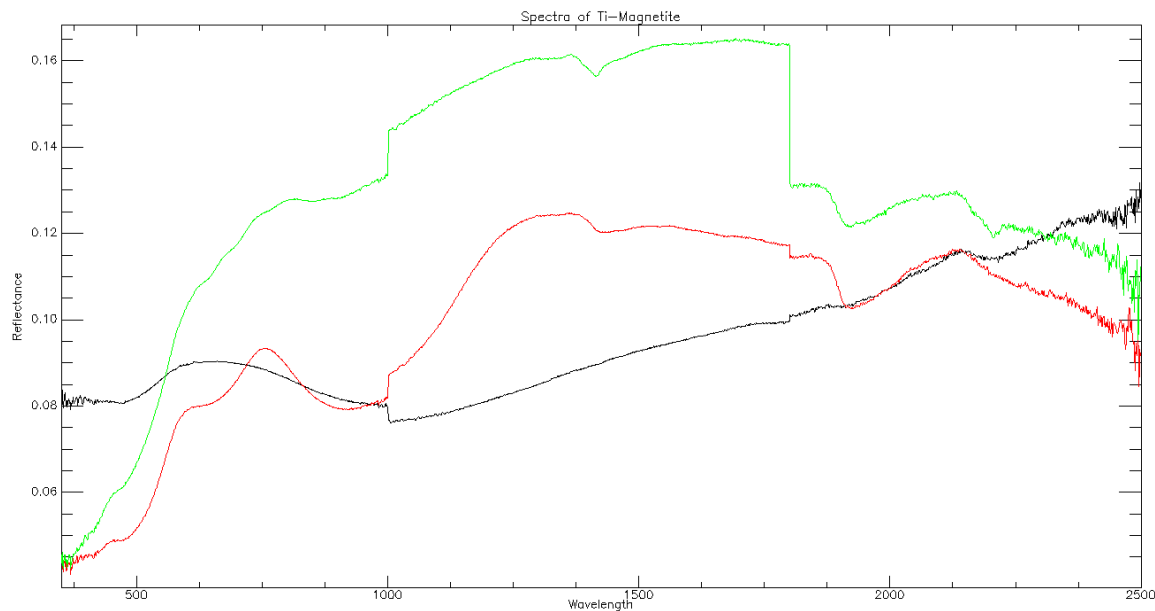
Figure 4.5 Spectral curves of fresh (black), weathered (red) and highly weathered (green) Magnetitite.

There was a minor absorption feature at 414nm. Although relatively small and dominated by a lot of noise, this absorption feature was more prominent in weathered and highly weathered samples. Also, these samples occurred at a lower reflectance (0.82 for weathered and 0.83 for highly weathered) than for fresh samples (0.94).

On the continuum-removed spectra, all samples of Mambulu magnetitite displayed an absorption feature at 460-515nm (Figure 4.6). For fresh samples the absorption centre was at 474nm; for weathered samples at 484 and 491nm; and for highly weathered samples at 476, 486 and 491nm. Again, the absorption features for weathered and highly weathered magnetitite were at a much lower reflectance (0.77 and 0.82) than for fresh magnetitite (0.92).
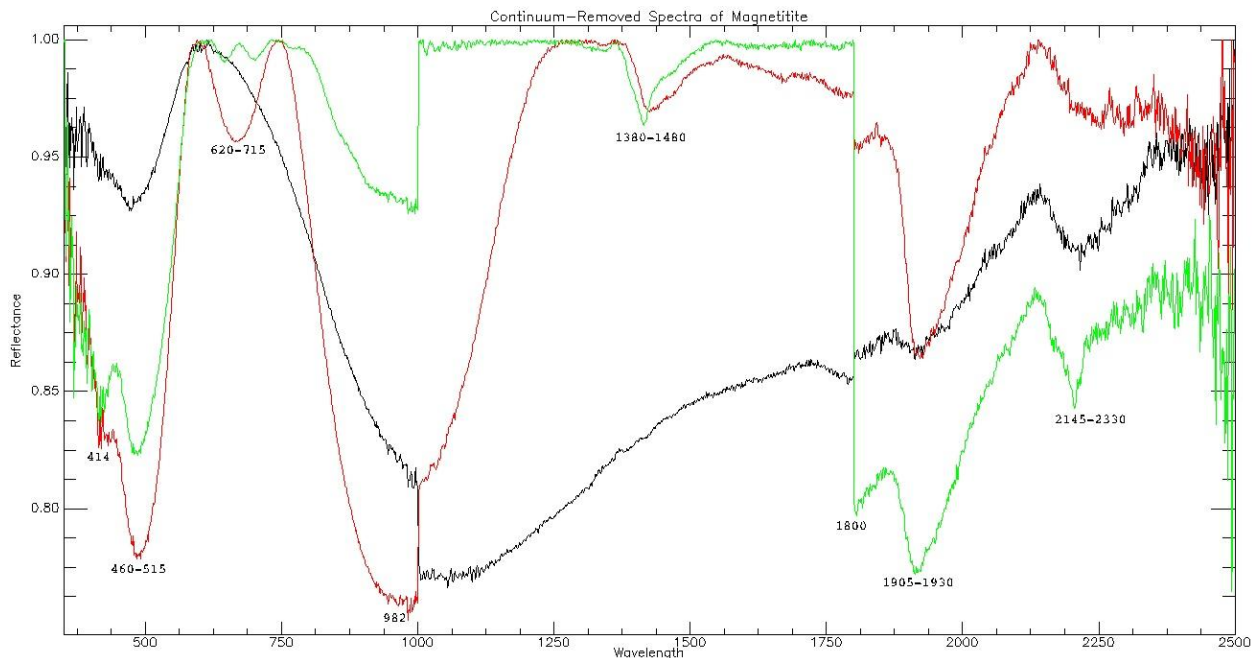
Figure 4.6 Continuum-removed spectra of fresh (black), weathered (red) and highly weathered (green) magnetitite.

Both weathered and highly weathered samples showed an absorption feature at 620-715nm. In this range, absorption was most pronounced for the weathered samples but displayed as a minor double absorption feature for the highly weathered magnetitite. The more pronounced absorption for weathered samples was deeper than the doublet for highly weathered samples. The absorption

centres were at 663nm (at 0.95 reflectance for weathered), 646nm and 701nm (at 0.99 reflectance for highly weathered). The fresh samples showed no absorption in this range.

There were minor absorptions at 982nm for all samples. Raja *et al* (2010), determined an absorption feature at 0.9µm (900nm) for magnetite quartzite. The absorptions for Mambulu magnetitite at this wavelength were minor yet distinct. All, however, occurred at varied reflectance values, increasing in reflectance from weathered (0.75) to fresh (0.80) to highly weathered (0.92).

Again, just the weathered and highly weathered spectra showed an absorption feature at 1380-1480nm which occurred at a very high reflectance (0.96). The centre for this absorption feature was at 1415nm for highly weathered samples and at 1425nm for weathered samples. There was no absorption in this region for the fresh samples.

All spectra showed a vertical absorption at 1800nm. The deepest of these was for highly weathered samples followed by weathered samples and then a very small absorption for fresh samples.

A deep absorption occurred at 1905-1930nm. The absorption feature was more distinct for weathered and highly weathered samples of which the former was the deepest and most distinct. Also, the feature for weathered samples was at a higher reflectance (0.86) than for highly weathered samples (0.77). This feature has minor doublet centre at 1914 and 1917nm for both weathered and highly weathered spectra. This absorption feature was not present in fresh samples.

There was a 2145-2330nm absorption feature for only fresh and highly weathered samples. The centres, which were distinct for the fresh and highly weathered samples, were at 2205nm (for highly weathered samples at 0.84 reflectance) and 2216nm (for fresh samples at 0.90 reflectance). The feature was not noticeable for weathered samples because of excess noise for those samples in that region.

4.2.5 MEDIUM-GRAINED PYROXENITE

Medium-grained pyroxenite had low reflectance. The spectra of both fresh and weathered samples ranged between 0.04-0.19 (Figure 4.7). Reflectance values for fresh samples increased from the visible to the near-infrared region, where it became stable and remained at that level for the rest of the spectrum. Here, reflectance values ranged from 0.9 to ~0.16. For weathered samples, spectra rise gently throughout the visible and infrared region and reach a maximum in the shortwave infrared region. Reflectance values for these spectra increased from 0.04 to around 0.19.
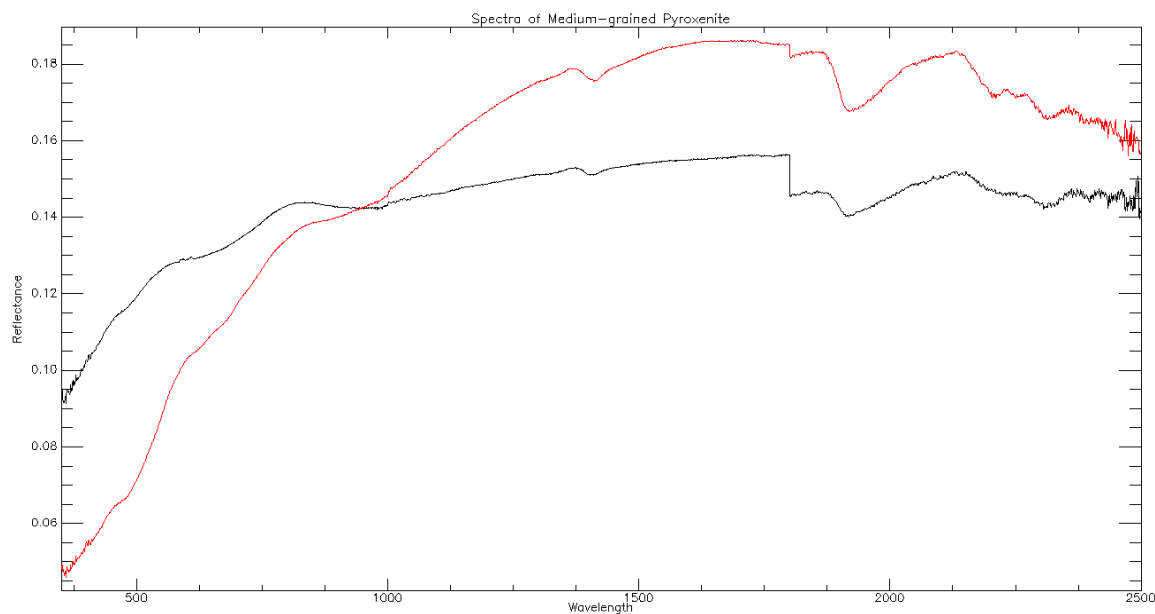
Figure 4.7 Spectral curves of fresh (black) and weathered (red) medium-grained pyroxenite.

The continuum-removed spectra for medium-grained pyroxenite are displayed in Figure 4.8. There was an absorption feature at 410-420nm which was more distinct in the weathered pyroxenite (Figure 4.8). The centres for this feature were at 413nm and 418nm. The feature was at a very high reflectance for fresh samples (0.98) and at a very low reflectance for weathered samples (0.88).

This was followed by a major absorption centred at 483nm. Again, this was more pronounced and much deeper for the weathered pyroxenite than for the fresh samples. Also, the feature was again at lower reflectance for weathered samples (0.86) than for fresh samples (0.99).

At 680nm, the absorption feature was more distinct and narrow for weathered samples than for fresh samples. Both absorptions occurred at the same reflectance (0.97).

The absorption feature at 977-993nm was present for both fresh and weathered samples. Although this feature was characterized by noise, a minor yet distinct absorption centre was noticed at 979nm for both fresh and weathered samples. These absorptions occurred at 0.969 for fresh samples and at 0.957 for weathered samples.
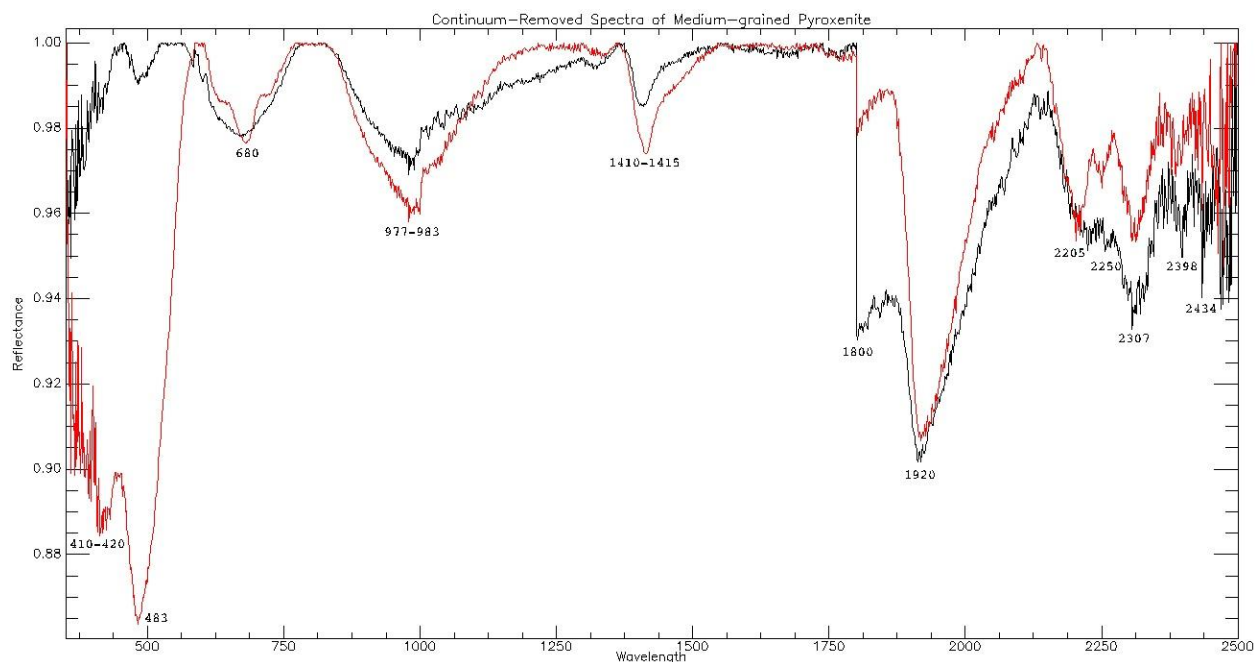
Figure 4.8 Continuum-removed spectra for fresh (black) and weathered (red) medium-grained pyroxenite.

The 1410-1415nm absorption feature had a slightly broader centre. Here, spectra for weathered samples of medium-grained pyroxenite were deeper than for fresh samples. These features occupied the same reflectance range (0.97-0.99) as the 680nm feature discussed above.

There is a prominent absorption feature, for both fresh and weathered spectra, at 1800nm as evidenced by a vertical drop in the spectral curves on Figure 4.8. This straight vertical dropped from 0.99 reflectance to 0.93 for fresh and to 0.98 for weathered samples.

A major absorption was present at 1920nm. It displayed as a very deep and narrow feature for both fresh and weathered samples of medium-grained pyroxenite. This feature occupied a much larger reflectance range (0.90-0.98) than all the other absorption features for medium-grained pyroxenite. Also, both fresh and weathered samples shared a very similar shape and reflectance position to each other, at this absorption.

After the 1920nm absorption, there were three minor, yet distinct absorptions at 2205, 2250, 2307nm. All three features were characterized by noise, but had very distinct absorption centres. The fresh and weathered spectra for 2205nm feature overlapped each other, showing that there was very little difference in their reflectance (0.95 for both fresh and weathered). For the 2250nm and 2307nm features weathered spectra occurred at a slightly higher reflectance (0.96 and 0.95 respectively) than fresh samples (0.95 and 0.93).

There were also a further two, very noisy, less distinct, absorptions at 2400 and 2430nm. Although very noisy, detailed study of the curves confirmed that these two absorption features had centres at 2398nm (at 0.94 reflectance for fresh and 0.97 for weathered) and 2434nm (at 0.94 reflectance for fresh and 0.96 for weathered). These wavelengths were considered because both were noticeable as absorptions.

4.2.6 COARSE-GRAINED PYROXENITE

Spectra for coarse-grained pyroxenite were similar to medium-grained spectra. They covered a reflectance range from 0.03 to 0.22 (Figure 4.9). However, the curves of these spectra varied in that they increased in reflectance at a steeper gradient than medium-grained samples. Fresh coarse-grained pyroxenite spectra ranged from 0.1 to 0.2. Weathered coarse-grained pyroxenite covered a reflectance range between 0.03 and 0.22. Both fresh and weathered samples increased in reflectance from the visible to the shortwave infrared to 1800nm and 1855nm respectively. Also, absorption features for coarse-grained samples were more pronounced than for medium-grained samples.
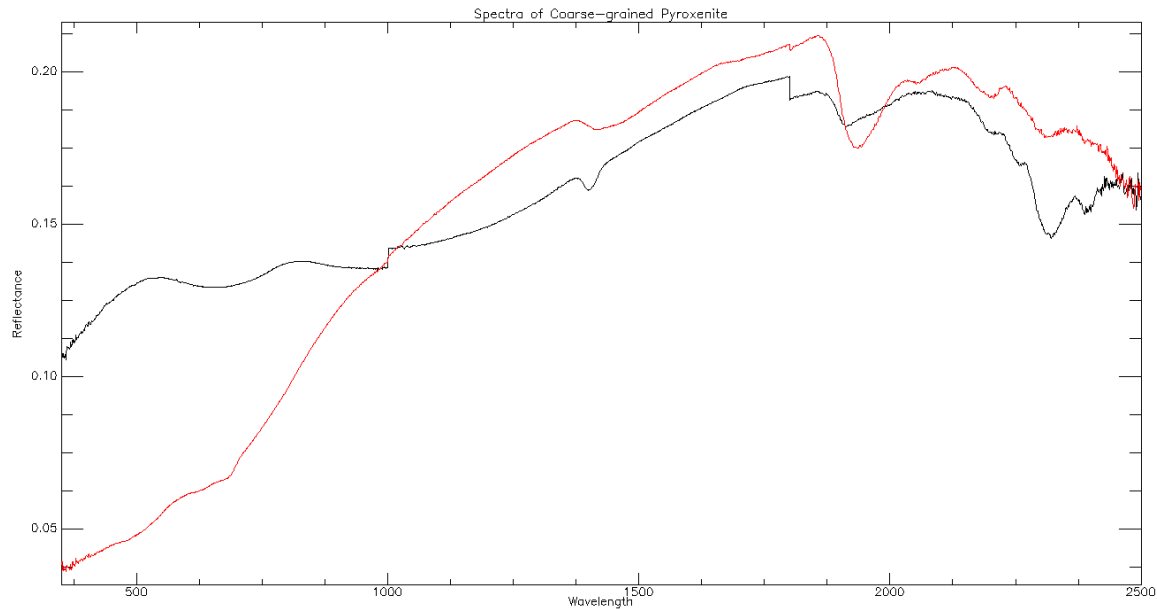
Figure 4.9 Spectral curves of fresh (black) and weathered (red) coarse-grained pyroxenite.

From Figure 4.10, it can be seen that a double absorption feature, for weathered samples, occurred at 460-727nm with the centres at 511nm (at 0.76 reflectance) and 680nm (at 0.73 reflectance). Fresh samples in this range displayed only a single, relatively broader absorption feature centred at around 711nm (at 0.91 reflectance).

Both fresh and weathered spectra displayed a very small absorption at 979nm (at 0.89 for fresh samples and 0.98 for weathered) followed by a larger one at 1000nm. This was more pronounced for fresh samples. Water absorption occurred as a narrow absorption feature at 1401nm for fresh samples (0.90), and as a broader feature at 1422nm for weathered samples (0.96).

The absorption feature at 1800nm was present in both fresh and weathered samples. The water absorption feature at 1900nm occurred at 1913nm in fresh samples and at 1930nm for weathered samples. Although very narrow for both spectra, it was very deep for weathered samples, compared to fresh samples, covering a very large reflectance range (0.83-0.99).

A minor absorption occurred at 2203nm for both samples at very high reflectance (0.96 for fresh and 0.97 for weathered). Another minor absorption occurred at 2258nm (at 0.92 reflectance) but was predominant only in fresh coarse-grained pyroxenite.
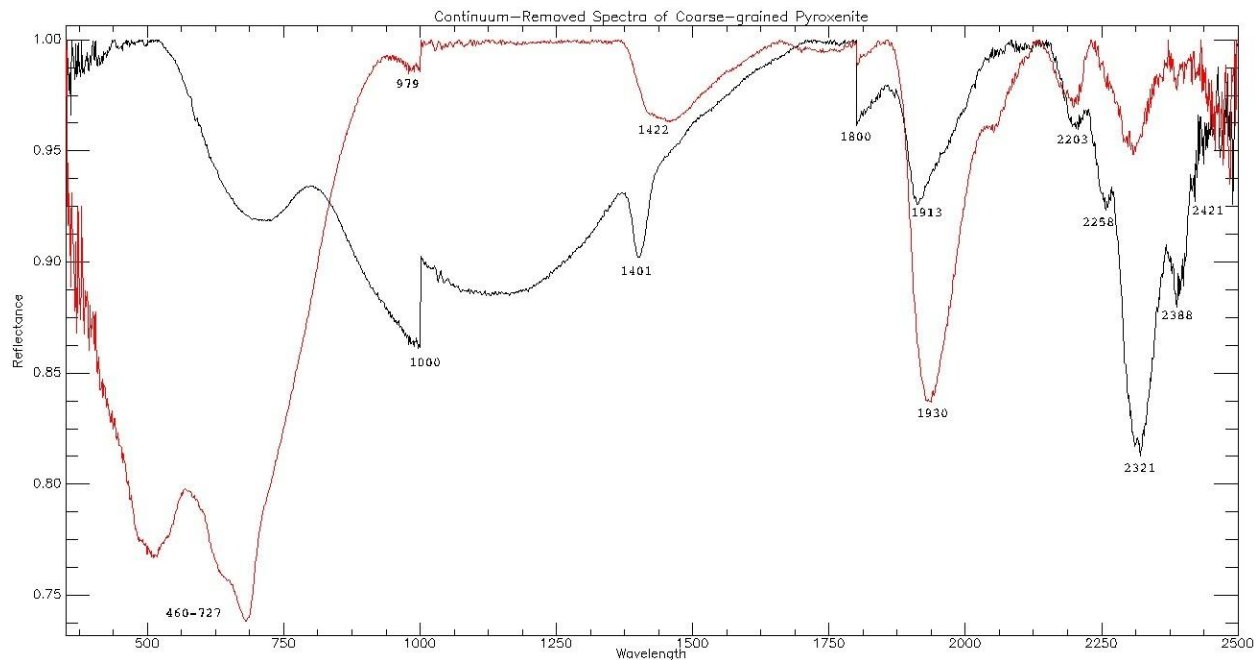
Figure 4.10 Continuum-removed spectra for fresh (black) and weathered (red) coarse-grained pyroxenite.

These minor absorptions were followed by a very deep absorption (more pronounced in fresh samples) at 2321nm. This absorption was much larger and deeper for fresh samples. It also covered a much larger reflectance range (0.81-0.90) than the features for weathered samples (0.95-0.98).

A few absorptions followed, but these are hard to distinguish in figure 4.10. There was a minor absorption at 2388nm which was again more prevalent in spectra for fresh samples (0.87), but also distinguishable in weathered samples (0.97). This was followed by a very minor absorption at 2421nm which was again more distinct in fresh spectra (0.92). This 2421nm feature was a mirror of the 2258 feature, in that it flanks the 2321nm at a very similar reflectance (0.92).

The reflectance spectra from the rock samples collected from the Mambulu Complex were compared to reference spectra from other spectral libraries; specifically rock spectra from the Johns Hopkins University (JHU) spectral library, and mineral spectra from the Jet Propulsion Laboratory (JPL) spectral library. This was done to ascertain whether spectra of the rocks from

the Mambulu Complex were of a good enough standard and also to see if absorption features found here matched those of well known and widely used spectral libraries. Both spectral libraries are part of the ENVI remote sensing software. Most of these libraries measured spectra in micrometers (µm) where 1µm = 1000nm.

Fine-grained anorthosite from the JHU spectral library showed absorption features at 0.46, 0.59, 0.67, 0.7, 0.82, 0.94, 1.04, 1.11, 1.2, 1.26, 1.36, 1.4, 1.6, 1.76, 1.83, 1.86, 1.89, 1.9, 2.19, 2.25, 2.34µm. Coarse-grained anorthosite from JHU spectral library had absorption features at 0.48, 1.11, 1.13, 1.4, 1.46, 1.75, 1.81, 1.9, 1.94, 2.2, 2.23, 2.25, and 2.33µm. Pure anorthite from the JPL mineral spectral library showed absorption features at 0.78, 0.88, 1.14, 1.22, 1.27, 1.32, 2.18, 2.25, 2.34, and 2.46µm. anorthosite from the Mambulu Complex showed absorption features at 480-490, 592, 603, 608, 627-726, 765, 1410, 1905-1955, 2200, 2250 and 2330nm. All absorption features from the Mambulu anorthosite (except the 603 and 608nm) match those of the JHU and JPL spectral libraries. The 603 and 608nm anomalies could be due to the minor differences in composition of the anorthosite from the Mambulu Complex compared to those used for the reference data.

Gabbro from the JHU spectral library had absorptions at 0.55, 0.97, 1.01, 1.08, 1.48, 2.3, 2.4µm. Leuco-gabbro absorption features were observed at 481, 950-1010, 1407, 1917, 2206, 2252, and 2300-2340nm. Similarities occur at 950-1010nm and 2300-2340nm with some correlation at 1407nm ($\equiv$1.48µm) and 2252nm. The discrepancies between the other absorption value is presumably linked to the difference in mineral composition between the JHU gabbro and the leuco-gabbro from the Mambulu Complex.

Magnetite from the JPL spectral library showed absorptions at 1.02, 1.06, 1.19, 1.5, 1.67, 2.08, 2.15, 2.2 and 2.32µm. The JPL spectral library also contained spectra of titanite which showed absorption features at 0.46, 0.62, 1.46, 2.2, 2.25 and 2.4µm. Titanite is a mineral titanium-calcium silicate ($CaTiSiO_4$) also known as the mineral sphene. Thus the link between the JPL titanite and magnetitite from the Mambulu Complex is the presence of the element titanium in the magnetite. Magnetitite from the Mambulu Complex displayed absorption features at 414, 460-515, 620-715, 982, 1380-1480, 1800, 1905-1930 and 2145-2330nm. Of these, the 460-515

and the 620-715nm features match the titanite spectra and the 2145-2303nm feature matched both the magnetite and titanite spectra. The differences here are attributed to the differences in composition.

The above spectral analyses showed that spectral analyses of the rocks from the Mambulu Complex were of a good standard and matched the JHU and JPL spectra for similar rocks. The absorption features for the Mambulu samples were correctly determined when matched against the well-known JHU and JPL spectra. The next step is to determine whether the rocks from the Mambulu Complex are significantly different from each other,

4.3 COMPARATIVE ANALYSIS OF REFLECTANCE SPECTRA
4.3.1 ANORTHOSITE
At the 480-490nm absorption feature, for anorthosite, there were significant differences between the rocks. The centres for this double-absorption feature were at 483nm and 489nm. Fresh anorthosite was significantly different from all other rock types, including weathered anorthosite. For weathered samples, however, there was no significant difference between weathered anorthosite; and fresh leuco-gabbro. Weathered samples of anorthosite were significantly different from all other samples.

There was a significant difference between rock types at the 1410nm absorption. Fresh anorthosite was significantly different from all rock types except weathered anorthosite and weathered leuco-gabbro. This pattern was also evident for weathered anorthosite. It should also be noted that this absorption feature lies in close proximity to the 1400nm water absorption feature present in almost all rocks, and could have affected the spectral characteristics of this 1410nm absorption feature.

For the 1905-1955nm absorption feature, there was a significant difference between the rock types. The absorption centre for this feature was at 1915nm. Fresh anorthosite at this wavelength was significantly different from fresh leuco-gabbro; fresh, weathered and highly weathered Magnetitite; fresh and weathered medium-grained pyroxenite; and fresh weathered coarse-grained pyroxenite. Weathered anorthosite at the absorption centre was also significantly

different from fresh leuco-gabbro; fresh, weathered and highly weathered magnetitite; fresh and weathered medium-grained pyroxenite; and fresh and weathered coarse-grained pyroxenite. This trend is evident for all wavelengths in this absorption feature.

The 2200nm absorption feature showed significant differences between anorthosite and the various rock types. These differences were the same as for previous wavelengths, where fresh and weathered anorthosite was significantly different from all other rocks but not significantly different from each other and from weathered leuco-gabbro.

Significant differences between the rock types occurred at the 2250nm absorption feature. Again, the above-mentioned trend is present in this absorption feature, where both fresh and weathered anorthosite were significantly different from fresh leuco-gabbro; fresh, weathered and highly weathered magnetitite; fresh and weathered medium-grained pyroxenite; and fresh and weathered coarse-grained pyroxenite. There was no significant difference between fresh and weathered anorthosite, and both were not significantly different from weathered leuco-gabbro.

For the 2330nm absorption feature, there were significant differences between the rock types. But here, fresh and weathered anorthosites have no significant differences between them. They (fresh and weathered anorthosite) were significantly different from all other rock types.

The ANOVAs and Bonferroni tests revealed that fresh and weathered anorthosite were significantly different from all other rocks. It also revealed that they were not significantly different from each other at the 1410, 1915, 1905-1955, 2200, 2250 and 2330nm absorption features. The 480-490nm absorption feature was the only feature where fresh and weathered anorthosite were statistically significantly different from each other. Also, there was no significant difference between anorthosite (both fresh and weathered) and weathered leuco-gabbro at 1410, 1905-1955, 2200 and 2250nm. For the 480-490nm feature, fresh but not weathered anorthosite was significantly different from fresh leuco-gabbro.

Table 4.1 Summary of the results of Bonferroni tests to illustrate the statistically significant difference between anorthosite and the other rocks of the Mambulu Complex F=fresh material W=weathered material

Anorthosite												
Absorption feature	f/w	1	2	3	4	5	6	7	8	9	10	11
480-490	F		●	●	●	●	●	●	●	●	●	●
	W	●			●	●	●	●	●	●	●	●
1410	F			●		●	●	●	●	●	●	●
	W			●		●	●	●	●	●	●	●
1905-1955	F			●		●	●	●	●	●	●	●
	W			●		●	●	●	●	●	●	●
2200	F			●		●	●	●	●	●	●	●
	W			●		●	●	●	●	●	●	●
2250	F			●		●	●	●	●	●	●	●
	W			●		●	●	●	●	●	●	●
2330	F			●	●	●	●	●	●	●	●	●
	W			●	●	●	●	●	●	●	●	●

The black dots indicate significant difference; and numbers 1-11 correspond to fresh anorthosite, weathered anorthosite, fresh leuco-gabbro, weathered leuco-gabbro, fresh magnetitite, weathered magnetitite, highly weathered magnetitite, fresh medium-grained pyroxenite, weathered medium-grained pyroxenite, fresh coarse-grained pyroxenite, and weathered coarse-grained pyroxenite respectively.

The table above (Table 4.1) summarises the significant difference (represented by a black dot) of fresh (F) and weathered (W) anorthosite from the other rocks, in the Mambulu complex, at all the absorption wavelengths. It can be deduced that both fresh and weathered anorthosite were significantly different, at all absorption wavelengths, from all other Mambulu rocks except each other and weathered leuco-gabbro (column 4).

4.3.2 LEUCO-GABBRO

At the 481nm absorption feature there were significant spectral differences between the rock types. Fresh samples of leuco-gabbro were significantly different from fresh anorthosite; fresh, weathered and highly weathered magnetitite (column 5-7); weathered medium-grained pyroxenite (column 9); and weathered coarse-grained pyroxenite (column 11). Weathered samples are significantly different from fresh and weathered anorthosite; fresh, weathered and

highly weathered magnetitite; weathered medium-grained pyroxenite and weathered coarse-grained pyroxenite

The absorption feature in the range 950-1010nm had significant differences between the various rock types. At the 992nm absorption centre, both fresh and weathered samples were significantly different from fresh and weathered anorthosite; and fresh and weathered magnetitite. For the 995nm absorption feature, both fresh and weathered samples were again only significantly different from fresh and weathered anorthosite; and fresh and weathered magnetitite. The trend for the absorption feature in the range 950-1010nm confirms significant differences between leuco-gabbro (fresh and weathered) and anorthosite (fresh and weathered); and between leuco-gabbro and magnetitite (fresh and weathered), but not between leuco-gabbro and any of the other samples.

ANOVAs for the 1407nm absorption feature showed that there were significant differences between the various rock types. These significant differences were between fresh samples of leuco-gabbro and fresh and weathered anorthosite; weathered leuco-gabbro; and fresh magnetitite. Weathered leuco-gabbro was significantly different from fresh leuco-gabbro; fresh, weathered, and highly weathered magnetitite; and all samples of medium- and coarse-grained pyroxenite.

At the 1917nm absorption feature there were significant differences between the various rock types. Fresh leuco-gabbro was significantly different from fresh and weathered anorthosite; weathered leuco-gabbro; and fresh and weathered magnetitite. Weathered samples of leuco-gabbro were significantly different from fresh leuco-gabbro; fresh, weathered and highly weathered magnetitite; fresh and weathered medium-grained pyroxenite; and fresh and weathered coarse-grained pyroxenite.

The 2206nm absorption feature had significant differences between the various rock types. For this absorption feature, fresh leuco-gabbro was only significantly different from fresh and weathered anorthosite; and weathered leuco-gabbro. Weathered leuco-gabbro was significantly

different from fresh leuco-gabbro; fresh, weathered and highly weathered magnetitite; and fresh and weathered medium-grained pyroxenite.

For the 2252nm absorption feature, there were significant differences between the various rock types. Fresh samples of leuco-gabbro were significantly different from fresh and weathered anorthosite; and weathered leuco-gabbro. Weathered leuco-gabbro was significantly different from fresh leuco-gabbro; fresh, weathered and highly weathered magnetitite; and fresh medium-grained pyroxenite.

At the 2320nm absorption feature, fresh leuco-gabbro was significantly different from fresh and weathered anorthosite; and weathered leuco-gabbro only. Weathered leuco-gabbro was significantly different from fresh and weathered anorthosite; fresh leuco-gabbro; and fresh, weathered and highly weathered magnetitite.

There were significant differences between the various rock types at the 2300-2340nm absorption feature. At the 2312nm absorption centre fresh samples of leuco-gabbro were significantly different from fresh and weathered anorthosite; and weathered leuco-gabbro. Weathered samples were significantly different from all rocks except the medium- and coarse-grained pyroxenite samples. At the 2321nm absorption centre fresh samples of leuco-gabbro were also significantly different from fresh and weathered anorthosite; and weathered leuco-gabbro. Weathered samples were again significantly different from all rocks except the medium- and coarse-grained pyroxenite. At the 2328nm absorption centre fresh samples of leuco-gabbro were significantly different from fresh and weathered anorthosite only. Weathered samples were significantly different from fresh leuco-gabbro; and from the medium- and coarse-grained pyroxenite. The significant difference for fresh and weathered leuco-gabbro against each other was not constant, and no pattern of significant difference was noticed across the absorption feature for this pair. The trend throughout this absorption feature was that fresh leuco-gabbro was always significantly different from fresh and weathered anorthosite. Weathered leuco-gabbro was also significantly different from fresh and weathered anorthosite, but in addition was significantly different from fresh, weathered and highly weathered magnetitite.

Table 4.2 Summary of the results of Bonferroni tests to illustrate the statistically significant difference between leuco-gabbro and the other rocks of the Mambulu Complex. F=fresh material W=weathered material

Leuco-gabbro												
Absorption feature	f/w	1	2	3	4	5	6	7	8	9	10	11
481	F	●				●	●	●		●		●
	W	●	●			●	●	●		●		●
950-1010	F	●	●			●	●					
	W	●	●			●	●					
1407	F	●	●		●	●	●					
	W			●		●	●	●	●	●	●	●
1917	F	●	●		●	●	●					
	W			●		●	●	●	●	●	●	●
2206	F	●	●		●							
	W			●		●	●	●	●	●		
2252	F	●	●		●							
	W			●		●	●	●	●			
2300-2340	F	●	●									
	W	●	●			●	●	●				
2385	F	●	●		●							
	W	●	●	●		●	●	●				

The black dots indicate significant difference; and numbers 1-11 correspond to fresh anorthosite, weathered anorthosite, fresh leuco-gabbro, weathered leuco-gabbro, fresh magnetitite, weathered magnetitite, highly weathered magnetitite, fresh medium-grained pyroxenite, weathered medium-grained pyroxenite, fresh coarse-grained pyroxenite, and weathered coarse-grained pyroxenite respectively.

At the 2385nm absorption feature fresh and weathered samples of leuco-gabbro were found to be significantly different from each other. All other differences were as determined at the 2300-2340nm absorption feature i.e. fresh samples of leuco-gabbro were significantly different from fresh and weathered anorthosite whereas weathered samples of leuco-gabbro were significantly different anorthosite (fresh and weathered) as well as magnetitite (fresh, weathered and highly weathered).

Table 4.2 provides a summary of the significant difference (represented by a black dot) of fresh (F) and weathered (W) leuco-gabbro from the other rocks, in the Mambulu complex, at all the

absorption wavelengths. Here, the significance of leuco-gabbro from the other rocks was variable. The only major patterns were significant differences between fresh leuco-gabbro and fresh anorthosite; and significant differences between weathered leuco-gabbro and weathered and highly weathered magnetitite at all absorption features

4.3.3 MAGNETITITE

At the 414nm absorption wavelength there were significant differences between the various rock types. For fresh magnetitite these significant differences occurred between the fresh samples and fresh and weathered anorthosite; fresh leuco-gabbro; weathered and highly weathered magnetitite; and all samples of medium- and coarse-grained pyroxenite. Weathered magnetitite was significantly different from fresh and weathered anorthosite; fresh and weathered leuco-gabbro; fresh magnetitite; fresh medium-grained pyroxenite and fresh coarse-grained pyroxenite. Highly weathered magnetitite was significantly different from fresh and weathered anorthosite; fresh and weathered leuco-gabbro; fresh magnetitite; fresh medium-grained pyroxenite and fresh coarse-grained pyroxenite. At this absorption wavelength it was determined that magnetitite samples (fresh, weathered and highly weathered) were significantly different from fresh and weathered anorthosite; fresh leuco-gabbro; fresh medium-grained pyroxenite; and fresh coarse-grained pyroxenite.

For the 460-515nm absorption feature there were significant differences between the various rock types throughout all wavelengths of the feature. At the 474 and 476nm centres, fresh magnetitite was significantly different from fresh and weathered anorthosite; fresh and weathered leuco-gabbro; weathered and highly weathered magnetitite; fresh medium-grained pyroxenite; and fresh and weathered coarse-grained pyroxenite. Weathered magnetitite was significantly different from fresh and weathered anorthosite; fresh and weathered leuco-gabbro; fresh magnetitite; fresh medium-grained pyroxenite; and fresh coarse-grained pyroxenite. Highly weathered magnetitite was significantly different from fresh and weathered anorthosite; fresh and weathered leuco-gabbro; fresh magnetitite; fresh medium-grained pyroxenite; and fresh and weathered coarse-grained pyroxenite. At the 484 and 486nm centres, fresh magnetitite was significantly different from fresh and weathered anorthosite; fresh and weathered leuco-gabbro; weathered magnetitite; fresh medium-grained pyroxenite; and fresh and weathered coarse-

grained pyroxenite. Weathered magnetitite was significantly different from fresh and weathered anorthosite; fresh and weathered leuco-gabbro; fresh magnetitite; fresh medium-grained pyroxenite; and fresh coarse-grained pyroxenite. Highly weathered magnetitite was significantly different from fresh and weathered anorthosite; fresh and weathered leuco-gabbro; fresh medium-grained pyroxenite; and fresh coarse-grained pyroxenite. At the 491nm centre, fresh magnetitite is significantly different from fresh and weathered anorthosite; fresh and weathered leuco-gabbro; weathered magnetitite; fresh medium-grained pyroxenite; and fresh and weathered coarse-grained pyroxenite. Weathered magnetitite was significantly different from fresh and weathered anorthosite; fresh and weathered leuco-gabbro; fresh magnetitite; fresh medium-grained pyroxenite; and fresh coarse-grained pyroxenite. Highly weathered magnetitite was significantly different from fresh and weathered anorthosite; fresh and weathered leuco-gabbro; fresh medium-grained pyroxenite; and fresh coarse-grained pyroxenite. The general trend at all wavelengths of the 460-515nm absorption feature was that fresh magnetitite was significantly different from fresh and weathered anorthosite; fresh and weathered leuco-gabbro; weathered and highly weathered magnetitite; fresh medium-grained pyroxenite; and fresh and weathered coarse-grained pyroxenite. Weathered magnetitite was significantly different from fresh and weathered anorthosite; fresh and weathered leuco-gabbro; fresh magnetitite; fresh medium-grained pyroxenite; and fresh coarse-grained pyroxenite. Highly weathered magnetitite was significantly different from fresh and weathered anorthosite; fresh and weathered leuco-gabbro; fresh medium-grained pyroxenite; and fresh coarse-grained pyroxenite

At the 620-715nm absorption feature there are significant differences between the various rock types. For the 646nm and 701nm minor doublet centres, fresh magnetitite was significantly different from fresh and weathered anorthosite; fresh and weathered leuco-gabbro; fresh medium-grained pyroxenite and fresh coarse-grained pyroxenite. Weathered samples at these centres were significantly different from fresh and weathered anorthosite; fresh and weathered leuco-gabbro; fresh medium-grained pyroxenite and fresh coarse-grained pyroxenite. Highly weathered samples were only significant different from fresh and weathered anorthosite and weathered coarse-grained pyroxenite. For the 663nm minor doublet centre fresh magnetitite was significantly different from fresh and weathered anorthosite; fresh and weathered leuco-gabbro; fresh medium-grained pyroxenite and fresh coarse-grained pyroxenite. Weathered magnetitite

also significantly different from fresh and weathered anorthosite; fresh and weathered leuco-gabbro; fresh medium-grained pyroxenite and fresh coarse-grained pyroxenite. Highly weathered magnetitite was significantly different from fresh and weathered anorthosite and weathered coarse-grained pyroxenite. The above trend was significant throughout the absorption features for both weathered and highly weathered magnetitite, and for most wavelengths for fresh magnetitite.

There were significant differences between the rock types at the 982nm absorption feature. Fresh magnetitite was significantly different from fresh and weathered anorthosite; fresh and weathered leuco-gabbro; highly weathered magnetitite; fresh and weathered medium-grained pyroxenite; and fresh and weathered coarse-grained pyroxenite. Weathered magnetitite was significantly different from fresh and weathered anorthosite; fresh and weathered leuco-gabbro; highly weathered magnetitite; fresh and weathered medium-grained pyroxenite; and fresh and weathered coarse-grained pyroxenite. Highly weathered samples of magnetitite were significantly different from fresh and weathered anorthosite; and fresh and weathered magnetitite.

For the 1380-1480nm absorption feature there were significant differences between the various rock types. At the 1415nm absorption centre fresh magnetitite was significantly different from fresh and weathered anorthosite; fresh and weathered leuco-gabbro; highly weathered magnetitite; fresh and weathered medium-grained pyroxenite; and fresh and weathered coarse-grained pyroxenite. Weathered samples were significantly different from fresh and weathered anorthosite; weathered leuco-gabbro; weathered medium-grained pyroxenite; and weathered coarse-grained pyroxenite. Highly weathered magnetitite was significantly different from fresh and weathered anorthosite; weathered leuco-gabbro; and fresh magnetite. For the 1425nm absorption centre, fresh magnetitite was significantly different from fresh and weathered anorthosite; fresh and weathered leuco-gabbro; highly weathered magnetite; fresh and weathered medium-grained pyroxenite; and fresh and weathered coarse-grained pyroxenite. Weathered samples were significantly different from fresh and weathered anorthosite; fresh and weathered leuco-gabbro; weathered medium-grained pyroxenite; and weathered coarse-grained pyroxenite. Highly weathered magnetitite was significantly different from fresh and weathered anorthosite;

weathered leuco-gabbro; and fresh magnetite. This trend was present throughout the absorption feature.

At the1800nm absorption wavelength, there were significant differences between the various rock types. Fresh samples of magnetitite were significantly different from fresh and weathered anorthosite; fresh and weathered leuco-gabbro; weathered medium-grained pyroxenite; and fresh and weathered coarse-grained pyroxenite. Weathered samples were significantly different from fresh and weathered anorthosite; fresh and weathered leuco-gabbro; weathered medium-grained pyroxenite; and fresh and weathered coarse-grained pyroxenite. Highly weathered samples of magnetitite were significantly different from fresh and weathered anorthosite; and weathered leuco-gabbro.

The 1905-1930nm absorption feature had significant differences between the various rock types. For the 1914nm and 1917nm absorption wavelengths, fresh samples of magnetitite were significantly different from fresh and weathered anorthosite; fresh and weathered leuco-gabbro; weathered medium-grained pyroxenite; and fresh and weathered coarse-grained pyroxenite. Weathered samples, at both wavelengths, were also significantly different from fresh and weathered anorthosite; fresh and weathered leuco-gabbro; weathered medium-grained pyroxenite; and fresh and weathered coarse-grained pyroxenite. Highly weathered samples were significantly different from fresh and weathered anorthosite; and weathered leuco-gabbro. However, at the 1917nm wavelength, highly weathered magnetitite was also significantly different from fresh coarse-grained pyroxenite.

Significant differences occurred between rocks at the 2145-2330nm absorption feature. At the 2205nm centre, fresh magnetitite was significantly different from fresh and weathered anorthosite; weathered leuco-gabbro; weathered medium-grained pyroxenite; and fresh and weathered coarse-grained pyroxenite. Weathered magnetitite was significantly different from fresh and weathered anorthosite; weathered leuco-gabbro; weathered medium-grained pyroxenite; and fresh and weathered coarse-grained pyroxenite. Highly weathered samples were

Table 4.3 Summary of the results of Bonferroni tests to illustrate the statistically significant difference between magnetitite and the other rocks of the Mambulu rocks. F=fresh material W=weathered material H=highly weathered material

Magnetitite												
Absorption feature	f/w/h	1	2	3	4	5	6	7	8	9	10	11
414	F	●	●	●			●	●	●	●	●	●
	W	●	●	●	●	●			●		●	
	H	●	●	●	●	●			●		●	
460-515	F	●	●	●	●		●		●		●	●
	W	●	●	●	●	●			●		●	
	H	●	●	●	●				●		●	
620-715	F	●	●	●	●				●		●	
	W	●	●	●	●				●		●	
	H	●	●									●
982	F	●	●	●	●			●	●	●	●	●
	W	●	●	●	●			●	●	●	●	●
	H	●	●									●
1380-1480	F	●	●	●	●			●	●	●	●	●
	W	●	●		●					●		●
	H	●	●		●	●						
1800	F	●	●	●	●					●	●	●
	W	●	●	●	●					●	●	●
	H	●	●		●							
1905-1930	F	●	●	●	●					●	●	●
	W	●	●	●	●					●	●	●
	H	●	●		●							
2145-2330	F	●	●		●					●	●	●
	W	●	●		●					●	●	●
	H	●	●		●						●	●

The black dots indicate significant difference; and numbers 1-11 correspond to fresh anorthosite, weathered anorthosite, fresh leuco-gabbro, weathered leuco-gabbro, fresh magnetitite, weathered magnetitite, highly weathered magnetitite, fresh medium-grained pyroxenite, weathered medium-grained pyroxenite, fresh coarse-grained pyroxenite, and weathered coarse-grained pyroxenite respectively.

significantly different from fresh and weathered anorthosite; weathered leuco-gabbro; and fresh and weathered coarse-grained pyroxenite. For the 2216nm absorption wavelength, fresh

magnetitite was significantly different from fresh and weathered anorthosite weathered leuco-gabbro; weathered medium-grained pyroxenite; and fresh and weathered coarse-grained pyroxenite. Weathered samples were significantly different from fresh and weathered anorthosite; weathered leuco-gabbro; weathered medium-grained pyroxenite; and fresh and weathered coarse-grained pyroxenite. Highly weathered magnetitite was significantly different from fresh and weathered anorthosite; weathered leuco-gabbro; and fresh and weathered coarse-grained pyroxenite. This was the trend throughout this absorption feature.

Table 4.3 provides a summary of the significant difference (represented by a black dot) of fresh (F), weathered (W) and highly weathered (H) magnetitite from the other rocks from the Mambulu Complex, at all the absorption wavelengths. Magnetitite was seen to be significantly different from both fresh and weathered anorthosite at all absorption wavelengths. Fresh and weathered samples of magnetitite were significantly different from fresh leuco-gabbro at all absorption s except the 2145-2330nm feature. All samples (except fresh at 414nm; and highly weathered at 620-715nm and 982nm) were significantly different from weathered leuco-gabbro at all wavelengths. Taking into account that image analysis uses surface reflectance, it should be noted that weathered magnetitite was significantly different from all the rocks at the 982nm absorption wavelength.

4.3.4 MEDIUM-GRAINED PYROXENITE

There were significant differences between the various rock types for 410-420nm absorption feature. For both the 413nm and 418nm absorption centres, fresh samples of medium-grained pyroxenite were significantly different from fresh anorthosite; fresh leuco-gabbro; fresh, weathered and highly weathered magnetitite; weathered medium-grained pyroxenite and weathered coarse-grained pyroxenite. Also for both absorption centres, weathered samples of medium-grained pyroxenite were significantly different from fresh and weathered anorthosite; fresh and weathered leuco-gabbro; fresh magnetitite; fresh medium-grained pyroxenite; fresh and weathered coarse-grained pyroxenite.

At the 483nm absorption wavelength, there were significant differences between the various rock types. Fresh medium-grained pyroxenite was significantly different from fresh and weathered

anorthosite; fresh, weathered and highly weathered magnetitite; weathered medium-grained pyroxenite; and weathered coarse-grained pyroxenite. Weathered medium-grained pyroxenite was significantly different from fresh and weathered anorthosite; fresh and weathered leuco-gabbro; weathered magnetitite; fresh medium-grained pyroxenite; and fresh and weathered coarse-grained pyroxenite.

There were significant differences between the rock types at the 680nm absorption wavelength. Fresh medium-grained pyroxenite was significantly different from fresh and weathered anorthosite; fresh and weathered magnetitite; and weathered coarse-grained pyroxenite. Weathered medium-grained pyroxenite was significantly different from fresh and weathered anorthosite; weathered leuco-gabbro; and weathered coarse-grained pyroxenite.

Significant differences occurred between the various rock types in the 977-993nm absorption feature. At the 979nm centre, fresh medium-grained pyroxenite was significantly different from fresh and weathered anorthosite; and fresh and weathered magnetitite. Weathered medium-grained pyroxenite, at the same centre, was also only significantly different from fresh and weathered anorthosite; and fresh and weathered magnetitite. This trend was prevalent at all wavelengths of this absorption feature.

There were significant differences between the various rock types at the 1410-1415nm absorption feature. At all wavelengths of this feature, fresh medium-grained pyroxenite was significantly different from fresh and weathered anorthosite; weathered leuco-gabbro; and fresh magnetitite. Weathered medium-grained pyroxenite, at all wavelengths of this feature, was significantly different from fresh and weathered anorthosite; weathered leuco-gabbro; fresh and weathered magnetitite.

At the 1800nm absorption feature, there were significant differences between the various rock types. Fresh medium-grained pyroxenite was significantly different from fresh and weathered anorthosite; and weathered leuco-gabbro. Weathered medium-grained pyroxenite was significantly different from fresh and weathered anorthosite; weathered leuco-gabbro; and fresh and weathered magnetitite.

There were significant differences between the carious rock types at the 1920nm absorption feature. Fresh medium-grained pyroxenite, at this wavelength, was significantly different from fresh and weathered anorthosite; and weathered leuco-gabbro. Weathered medium-grained pyroxenite was significantly different from fresh and weathered anorthosite; weathered leuco-gabbro; and fresh and weathered magnetitite.

For the 2205nm absorption feature, there were significant differences between the various rock types. Fresh medium-grained pyroxenite was significantly different from fresh and weathered anorthosite; and weathered leuco-gabbro. Weathered medium-grained pyroxenite was significantly different from fresh and weathered anorthosite; weathered leuco-gabbro; and fresh and weathered magnetitite.

Significant differences occurred between the rock types at the 2250nm absorption feature. Fresh medium-grained pyroxenite was significantly different from fresh and weathered anorthosite; and weathered leuco-gabbro. Weathered medium-grained pyroxenite was significantly different from fresh and weathered anorthosite; and fresh and weathered magnetitite.

There were significant differences between the various rock types at the 2307nm absorption feature. Fresh medium-grained pyroxenite was significantly different from fresh and weathered anorthosite. Weathered medium-grained pyroxenite was significantly different from fresh and weathered anorthosite; and weathered magnetitite.

At the 2398nm absorption feature, there were significant differences between the various rock types. Fresh medium-grained pyroxenite was only significantly different from fresh and weathered anorthosite. Weathered medium-grained pyroxenite was significantly different from fresh and weathered anorthosite; and weathered magnetitite.

For the 2434nm absorption feature, there were significant differences between rocks. Fresh medium-grained pyroxenite was significantly different from fresh and weathered anorthosite;

and weathered leuco-gabbro. Weathered medium-grained pyroxenite was significantly different from fresh and weathered anorthosite; and weathered magnetitite.

Table 4.4 Summary of the results of Bonferroni tests to illustrate the statistically significant difference between medium-grained pyroxenite and the other rocks of the Mambulu rocks. F=fresh material W=weathered material

Medium-grained pyroxenite												
Absorption feature	f/w	1	2	3	4	5	6	7	8	9	10	11
410-420	F	●		●		●	●	●		●		●
	W	●	●	●	●	●			●		●	●
483	F	●	●			●	●	●		●		●
	W	●	●	●	●		●		●		●	●
680	F	●	●			●	●					●
	W	●	●		●							●
977-993	F	●	●			●	●					
	W	●	●			●	●					
1410-1415	F	●	●		●	●						
	W	●	●		●	●	●					
1800	F	●	●		●							
	W	●	●		●	●	●					
1920	F	●	●		●							
	W	●	●		●	●	●					
2205	F	●	●		●							
	W	●	●		●	●	●					
2250	F	●	●		●							
	W	●	●			●	●					
2307	F	●	●									
	W	●	●				●					
2398	F	●	●									
	W	●	●				●					
2434	F	●	●		●							
	W	●	●				●					

The black dots indicate significant difference; and numbers 1-11 correspond to fresh anorthosite, weathered anorthosite, fresh leuco-gabbro, weathered leuco-gabbro, fresh magnetitite, weathered magnetitite, highly weathered magnetitite, fresh medium-grained pyroxenite, weathered medium-grained pyroxenite, fresh coarse-grained pyroxenite, and weathered coarse-grained pyroxenite respectively.

The significance of fresh (F) and weathered (W) medium-grained pyroxenite from the other Mambulu rocks was presented in Table 4.4. The only noticeable trend was that both fresh and weathered samples were significantly different from fresh and weathered anorthosite. Also, weathered samples, for all absorption features except 410-420nm and 680nm, were significantly different from weathered magnetitite. At the 410-420nm feature, weathered medium-grained pyroxenite was significantly different from the fresh samples of all other rocks.

4.3.5 COARSE-GRAINED PYROXENITE

For the 460-727nm absorption feature, there were significant differences between rocks. At the 511nm centre, fresh coarse-grained pyroxenite was significantly different from fresh and weathered anorthosite; fresh, weathered and highly weathered magnetitite; weathered medium-grained pyroxenite; and weathered coarse-grained pyroxenite. Also at this centre, weathered coarse-grained pyroxenite was significantly different from fresh and weathered anorthosite; fresh and weathered leuco-gabbro; fresh and highly weathered magnetitite; fresh and weathered medium-grained pyroxenite; and fresh coarse-grained pyroxenite. At the 680nm centre, fresh coarse-grained pyroxenite was significantly different from fresh and weathered anorthosite; fresh and weathered magnetitite; and weathered coarse-grained pyroxenite. Weathered coarse-grained pyroxenite, at this centre, was significantly different from fresh and weathered anorthosite; fresh and weathered leuco-gabbro; highly weathered magnetitite; fresh and weathered medium-grained pyroxenite; and fresh coarse-grained pyroxenite. At the 711nm centre, fresh coarse-grained pyroxenite was significantly different from fresh and weathered anorthosite; fresh and weathered magnetitite; and weathered coarse-grained pyroxenite. Also at this centre, weathered coarse-grained pyroxenite was significantly different from fresh and weathered anorthosite; fresh and weathered leuco-gabbro; highly weathered magnetitite; fresh and weathered medium-grained pyroxenite; and fresh coarse-grained pyroxenite. The trend throughout this feature showed that fresh coarse-grained pyroxenite was significantly different from fresh and weathered anorthosite; fresh and weathered magnetitite; and weathered coarse-grained pyroxenite. The trend also showed that weathered coarse-grained pyroxenite was significantly different from fresh and weathered anorthosite; fresh and weathered leuco-gabbro; highly weathered magnetitite; fresh and weathered medium-grained pyroxenite; and fresh coarse-grained pyroxenite.

There were significant differences at the 979nm absorption feature. Here, fresh coarse-grained pyroxenite was significantly different from fresh and weathered anorthosite; and fresh and weathered magnetitite. Weathered coarse-grained pyroxenite was also only significantly different from fresh and weathered anorthosite; and fresh and weathered magnetitite.

At the 1000nm absorption feature, there were significant differences between rocks. Fresh coarse-grained pyroxenite was significantly different from fresh and weathered anorthosite and fresh and weathered magnetitite. Weathered coarse-grained pyroxenite was significantly different from fresh and weathered anorthosite; and fresh and weathered magnetitite.

Significant differences occurred between rocks at the 1401nm absorption feature. Fresh coarse-grained pyroxenite was significantly different from fresh and weathered anorthosite; weathered leuco-gabbro; and fresh magnetitite. Weathered coarse-grained pyroxenite was significantly different from fresh and weathered anorthosite; weathered leuco-gabbro; and fresh and weathered magnetitite.

There were significant differences between rocks at the 1422nm absorption feature. Fresh samples of coarse-grained pyroxenite were significantly different from fresh and weathered anorthosite; weathered leuco-gabbro; and fresh magnetitite. Weathered samples of coarse-grained pyroxenite were significantly different from fresh and weathered anorthosite; weathered leuco-gabbro; and fresh and weathered magnetitite.

For the 1800nm absorption feature, there were significant differences between rocks. Fresh coarse-grained pyroxenite was significantly different from fresh and weathered anorthosite; weathered leuco-gabbro; and fresh and weathered magnetitite. Weathered coarse-grained pyroxenite was significantly different from fresh and weathered anorthosite; weathered leuco-gabbro; and fresh and weathered magnetitite.

At the 1913nm absorption feature, there were significant differences between rocks. Fresh coarse-grained pyroxenite was significantly different from fresh and weathered anorthosite; weathered leuco-gabbro; and fresh and weathered magnetitite. Weathered coarse-grained

pyroxenite was significantly different from fresh and weathered anorthosite; weathered leuco-gabbro; and fresh and weathered magnetitite.

Significant differences occurred between rocks at the 1930nm absorption feature. Fresh coarse-grained pyroxenite was significantly different from fresh and weathered anorthosite; weathered leuco-gabbro; and fresh, weathered and highly weathered magnetitite. Weathered coarse-grained pyroxenite was significantly different from fresh and weathered anorthosite; weathered leuco-gabbro; and fresh and weathered magnetitite.

There were significant differences between rocks at the 2203nm absorption feature. Fresh coarse-grained pyroxenite was significantly different from fresh and weathered anorthosite; and fresh, weathered and highly weathered magnetitite. Weathered coarse-grained pyroxenite was significantly different from fresh and weathered anorthosite; and fresh, weathered and highly weathered magnetitite.

For the 2258nm absorption feature, there were significant differences between rocks. Fresh samples of coarse-grained pyroxenite were significantly different from fresh and weathered anorthosite; and highly weathered magnetitite. Weathered samples of coarse-grained pyroxenite were significantly different from fresh and weathered anorthosite; and fresh, weathered and highly weathered magnetitite.

At the 2321nm absorption feature, there were significant differences between rocks. Fresh coarse-grained pyroxenite was only significantly different from fresh and weathered anorthosite. Weathered coarse-grained pyroxenite was significantly different from fresh and weathered anorthosite; and fresh, weathered and highly weathered magnetitite.

Significant differences occurred between rocks at the 2388nm absorption feature. Fresh coarse-grained pyroxenite was only significantly different from fresh and weathered anorthosite. Weathered coarse-grained pyroxenite was significantly different from fresh and weathered anorthosite; and fresh, weathered and highly weathered magnetitite.

Table 4.5 Summary of the results of Bonferroni tests to illustrate the statistically significant difference between coarse-grained pyroxenite and the other rocks of the Mambulu rocks. F=fresh material W=weathered material

Coarse-grained pyroxenite												
Absorption feature	f/w	1	2	3	4	5	6	7	8	9	10	11
460-727	F	●	●			●	●					●
	W	●	●	●	●			●	●	●	●	
979	F	●	●			●	●					
	W	●	●			●	●					
1000	F	●	●			●	●					
	W	●	●			●	●					
1401	F	●	●		●	●						
	W	●	●		●	●	●					
1422	F	●	●		●	●						
	W	●	●		●	●	●					
1800	F	●	●		●	●	●					
	W	●	●		●	●	●					
1913	F	●	●		●	●	●					
	W	●	●		●	●	●					
1930	F	●	●		●	●	●	●				
	W	●	●		●	●	●					
2203	F	●	●			●	●	●				
	W	●	●			●	●	●				
2258	F	●	●					●				
	W	●	●			●	●	●				
2321	F	●	●									
	W	●	●			●	●	●				
2388	F	●	●									
	W	●	●			●	●	●				
2421	F	●	●				●					
	W	●	●				●	●				

The black dots indicate significant difference; and numbers 1-11 correspond to fresh anorthosite, weathered anorthosite, fresh leuco-gabbro, weathered leuco-gabbro, fresh magnetitite, weathered magnetitite, highly weathered magnetitite, fresh medium-grained pyroxenite, weathered medium-grained pyroxenite, fresh coarse-grained pyroxenite, and weathered coarse-grained pyroxenite respectively.

There were significant differences between rocks at the 2421nm absorption feature. Fresh samples of coarse-grained pyroxenite were significantly different from fresh and weathered anorthosite; and weathered magnetitite. Weathered samples of coarse-grained pyroxenite were significantly different from fresh and weathered anorthosite; and weathered and highly weathered magnetitite.

Table 4.5 summarised the significant difference of fresh (F) and weathered (W) coarse-grained pyroxenite from the other Mambulu rocks. Both fresh and weathered samples were significantly different from fresh and weathered anorthosite at all absorption wavelengths. Weathered coarse-grained pyroxenite was significantly different from weathered magnetitite at all wavelengths, except the 460-727nm.

4.4 DISCUSSION

The data collected during the present study show that the rocks of the Mambulu Complex have significant spectral differences between them. Section 4.3 above, analysed each absorption feature to determine between which pairs of rocks these differences occurred. This section will provide reasons for these significant differences and also attempt to explain the processes that influence these significant differences.

A study was conducted by Sgavetti *et al* (2006), on the spectral behaviour of a suite of cumulates (predominantly norites and anorthosites) from the Bjerkreim-Sokndal Layered Intrusion in Norway. Rock modal composition of these cumulates mainly comprised plagioclase, ilmenite and Ca-poor pyroxene. Absorption bands diagnostic of pyroxene were near 0.9 and 1.8µm, and were attributed to Fe^{2+}/M2 site crystal field transitions. All samples measured showed that absorption band minima shifted toward larger wavelengths with increasing Fe^{2+} content in the octahedral M2 site.

In a similar study Pompilio *et al* (2007), deduced that weak absorption, in a typical anorthosite spectral curve, is centred between 622 and 715nm. Also, an electronic absorption occurs near 1260nm. Pyroxene, plagioclase and ilmenite (anhydrous minerals) show sharp and narrow vibrational absorptions occurring at the NIR wavelength range (Pompilio *et al*, 2007). These

were attributed to minerals derived from hydration and hydroxylation of the primary mineral phases (Pompilio *et al*, 2007). These bands occur at 1400, 1900, ~2200, ~2250 and ~2330nm and were evident throughout all samples of that series. All these absorptions were present in anorthosite from the Mambulu Complex and are therefore also attributed to the minerals derived from hydration and hydroxylation of the primary mineral phases.

Aarthy and Sanjeevi (2007), observed distinct absorption features, for anorthosite, in band 63 of a Hyperspectral Imager (HySI) instrument. This band corresponds to the 942.5nm to 946.25nm region of the electromagnetic spectrum. This absorption feature was not present in samples of the anorthosite from the Mambulu Complex. This may be attributed to the variation in composition of anorthosite from the Mambulu Complex.

A study was conducted by Anbazhagan and Arivazhagan (2010), in the Sittampundi Anorthosite complex, in the Tamil Nadu state of India. This is a layered igneous body dominated by relatively pure calcic anorthosite (An80-100) with less than 10% mafic minerals. The important minerals of these intrusions were plagioclase (anorthite, labradorite), pyroxene (augite, diopside), olivine and minor amounts of mafic minerals (Anbazhagan and Arivazhagan, 2010). After continuum removal, Anbazhagan and Arivazhagan (2010), determined major absorption features at 1000, 1100, 1200, 1410, 1920, 2200 and 2330nm. Of these, only the 1410, 1920, 2200 and 2330nm features were present in anorthosite from the Mambulu Complex. These absorption features are similar to those measured by Pompilio *et al* (2007) and are attributed to the minerals derived from hydration and hydroxylation of the primary mineral phases.

Anbazhagan *et al* (2012), identified a number of diagnostic absorption features in anorthosite and offered the following possible explanations for these features:
1. the Fe^{2+} and Fe^{3+} intervalance charge transfer absorptions near 770nm
2. olivine multiple component absorption at 1050nm
3. pyroxene absorption bands near 1000nm and 2000nm
4. plagioclase feldspar with >1% of FeO for the weak absorption at 1250-1300nm

The absorption feature at 765nm in the anorthosite from the Mambulu Complex may be linked to number 1 above.

Anbazhagan and Arivazhagan (2011), conducted a study to determine the suitability of terrestrial norite and gabbbro as reference spectra for remote lunar crust mapping. Absorption spectra of gabbro was observed at 378, 1200, 1407, 1790, 1912, 2205, 2262 and 2340nm. These spectra were also compared to reflectance spectra of gabbro collected from the spectral library at Johns Hopkins University, USA; and the absorption features for both matched (Anbazhagan and Arivazhagan, 2011). Of these, the 1407, 1917, 2206, 2252, 2320nm were observable in leuco-gabbro from the Mambulu Complex.

According to Qaid *et al* (2009), gabbro spectra show intense absorption features at 1400, 1900, 2340 and 2400nm which they attributed to the presence of molecules of OH, H_2O and CO_3^{-2} respectively. Leuco-gabbro from the Mambulu complex had similar absorptions at 1407, 1917, 2300-2340 and 2385. The 2300-2340nm absorption feature for leuco-gabbro encompasses the weak to moderate 2.33μm Fe.Mg-OH feature related to the minerals biotite and/or hornblende by Qaid *et al* (2009). Also, Qaid *et al* (2009), recorded intense absorption features at 2.05μm and 1.85μm and an absorption at 0.9μm which is attributed to the ferrous ion. The leuco-gabbro from the Mambulu Complex had a very strong absorption feature at 950-1010nm which is probably also due to the ferrous ion absorption band (Qaid *et al*, 2009).

Magnetitite and pyroxenite have not, to the author's knowledge, been studied for their spectral properties. The Mambulu rocks would also have slightly different compositions when compared to the same rocks from other localities, because of different modes of formation and presence of varying amounts of constituent minerals. It is, it is however, possible to classify rocks based on their spectral properties. Each mineral constituent of a rock influences the interaction of radiation with the rock and therefore influences the absorption characteristics of all rocks containing that mineral, in a very similar way. It is on this premise that the subsequent absorption wavelengths are discussed.

Atmospheric water bands are centred at 1.4 and 1.9μm (Goetz *et al*, 1985; Hauff, no date). These were present for all samples analysed but were characterized by noise. Although discussed above, both were eliminated as diagnostic absorption features.

The 1410nm feature measured for all samples was the same as spectra measured by Anbazhagan and Arivazhagan (2010) and Pompilio et al (2007). Anbazhagan and Arivazhagan (2010), attribute this absorption to OH/Mn^{3+} crystal transition.

The 1905-1955nm major absorption feature for anorthosite was also measured by Anbazhagan and Arivazhagan (2010) and Pompilio et al (2007). The cause of this absorption was attributed to ferrous iron/H_2O which is centred at 1915nm (Anbazhagan and Arivazhagan, 2010). This ferrous iron/ H_2O absorption feature was noted for anorthosite from the Mambulu Complex but in addition was also present in all spectra for leuco-gabbro, magnetitite, medium- and coarse-grained pyroxenite.

The absorption at 2200nm has been attributed to Al-OH absorption (Qaid et al, 2009; Anbazhagan and Arivazhagan, 2010). This Al-OH absorption feature was distinct for all rocks from the Mambulu Complex.

The 2250nm absorption feature is due to Mg-OH vibration spectra (Anbazhagan and Arivazhagan, 2010). This feature was present in anorthosite, and medium- and coarse-pyroxenite. The two absorption bands, for leuco-gabbro, at 2250 and 2320nm are attributed to hydroxyl bonds characteristic of gabbro spectra (Qaid et al, 2009).

In the visible to near-infrared range, mineral spectra are dominated by the presence or absence of transition metal ions such as Fe, Ni, Cr, etc. (van der Meer, 2004). In the SWIR region, the presence or absence of water and hydroxyl determine absorption features (van der Meer, 2004). The water molecule gives rise to overtones such as those seen in reflectance spectra of H_2O-bearing minerals. Hydroxyl ions are usually bound to Mg or Al. Overtones of the OH stretches occur near 1.4µm. while the combinations of H-O-H bend with the OH stretches influence absorption at about 1.9µm (van der Meer, 2004). More than one OH feature may be present because OH-groups normally occur in multiple crystallographic sites of a specific mineral and generally attached to metal ions (van der Meer, 2004). The combination of OH-stretch and metal-OH bend occurs near 2.2-2.3µm and is diagnostic of mineral composition (van der Meer).

Iron absorption-bands near 1 and 2μm shift as a function of Fe: (Fe +Mg) ratio Cloutis *et al*, 1986).

The main input variables of igneous rocks are temperature, pressure, water, oxygen, composition of the melt and gas fugacities (Sgavetti *et al*, 2006). The output is series of mineral phases, of which some are the solid solutions between two end members e.g. feldspar (Sgavetti *et al*, 2006). Magmatic rocks are therefore made up of complex chemical systems, and are constrained by specific physio-chemical conditions that affect composition, texture, crystal structure and degree of crystallinity (Sgavetti *et al*, 2006). Since the petrology and geochemistry affect the spectral signatures of rocks, spectral variability is intrinsic to the involved rock-forming process (Sgavetti *et al*, 2006). This results in genetically related rocks displaying 'systematic variations of spectral parameters as functions of systematic variations of petrographical and geochemical parameters' (Sgavetti *et al*, 2006: 144).

From the ANOVAs and Bonferroni tests it was deduced that all absorption features for all the rocks of the Mambulu Complex were significantly different from each other. Therefore, there are spectral features characteristic of each rock type and significant spectral differences between the different rocks in the Mambulu Complex. This can be explained by the fact that (excluding the magnetitite) although the rocks are composed of similar minerals their differences may be attributed to the compositions of these minerals and the ratios/abundances in which they are present.

It should be noted that this study focused on a specific suite of rocks for sample collection. For the four rock types chosen, spectra were measured for both fresh and weathered (highly weathered for magnetitite); and both medium- and coarse-grained for pyroxenite. In effect, this gave a total of 11 rock surfaces that were measured. The above analysis showed significant differences between all the rocks for all absorption features. However, there was much overlap among the different absorption features. These overlaps occurred mostly at absorptions where common minerals were present. After further analysis, the overlapping absorption features were eliminated. This was done to determine whether any of the rock samples from the Mambulu Complex contained unique absorption features, specific to only that rock. This left several

absorption features, for all rocks, that were significantly different from other rocks, both at specific wavelengths and reflectance values (Table 4.6).

Table 4.6 Table summarising diagnostic absorption bands of rocks of the Mambulu Complex

Rock Type	Diagnostic absorption features (nm)
Anorthosite	592, 603, 608, 765
Magnetitite	663, 2145-2330
Medium-grained pyroxenite	2398, 2434
Coarse-grained pyroxenite	511, 711, 1000, 2421

Anorthosite had diagnostic absorption features at 592, 603, 608 and 765nm. The diagnostic absorption features for magnetitite were at 663nm and 2145-2330nm. For medium-grained pyroxenite diagnostic absorption features occurred at 2398nm and 2434nm. The diagnostic absorption features for coarse-grained pyroxenite, however, were at 511, 711, 1000 and 2421nm.

Also, all absorption features for leuco-gabbro had some overlap with those of the other rock types, and were therefore eliminated. Hence, from the criteria used to determine the diagnostic absorption features for rocks from the Mambulu Complex, leuco-gabbro had no diagnostic absorption feature that did not overlap with absorption features of the other rocks.

The reason for the major overlaps may be attributed to the composition of the rocks. As mentioned earlier, absorption features are dependent on, amongst other factors, mineral composition. Taking into account that all the rocks of the Mambulu Complex were produced by the same magmatic event, there will be many similarities in their compositions. These similarities are shown by the overlap of absorption features across the spectrum.

The rock types of the Mambulu Complex are related in terms of mineral composition. Absorption features for the monominerallic rocks (anorthosite, magnetitite and pyroxenite) were compared to those of leuco-gabbro (which has a more varied mineral composition) to determine if this distinction affects the prominence of these absorption features. All absorption features for leuco-gabbro, however prominent they were, were identical in some way to the absorption features of one or more of the monominerallic rocks, e.g. the absorption features at 2315nm (fresh samples) 2325nm (weathered samples) were very prominent in leuco-gabbro. The same absorption features were, however, not prominent in the monominerallic rocks except for fresh samples of coarse-grained pyroxenite. The prominent absorption feature at 991nm for leuco-gabbro was present in all samples of magnetitite and pyroxenite, but was most prominent in weathered magnetitite. These examples show that the "strength" or prominence of absorption features is dependent on the composition (monominerallic versus more varied composition) of the rock types of the Mambulu Complex.

Grain size affects the amount of radiation scattered and absorbed by a mineral grain (Clark, 1999). Larger grains have a greater internal path where photons can be absorbed according to Beer's Law (Clark, 1999). Reflection from the surfaces and internal imperfections control scattering of radiation for these larger grains. Smaller grains, on the other hand, have proportionally more surface reflections compared to internal photon path lengths, i.e. the surface-to-volume ratio is a function of grain size (Clark, 1999). The absorption features for medium- and coarse-grained pyroxenite from the Mambulu Complex were compared to each other to determine the effects of grain size on these features. All samples are composed of the same basic minerals but have different grain sizes. Analysis showed that absorption features for coarse-grained samples were more prominent or 'deeper' than for medium-grained samples. This is most evident at the 511, 680, 1000, 1401, 1930 and 2321nm absorption features. It can therefore be concluded that grain size does affect the strength of absorption features of the rocks from the Mambulu Complex and by extension other igneous rocks.

The effects of weathering on Mambulu rocks have shown that fresh and weathered surfaces can be significantly different from each other. In the absence of vegetation and soil cover, even weathering products cover bedrock (Mather and Koch, 2011). Mather and Koch (2011) and

Younis *et al* (1997), indicate that characteristics of the spectral reflectance of rocks are determined by the mineralogy of the upper 50 µm, and weathering can significantly alter the observed spectral reflectance by producing a surface layer that is different in composition from the parent rock. Weathering causes rinds/crusts of altered minerals to form on the exposed surfaces of rocks. These new minerals are often significantly different (both chemically and mechanically) from the unweathered parent rock (Mather and Koch, 2011; Kaufmann *et al*, 2010; Younis *et al*, 1997). This new mineralogy means that spectral signatures derived from weathered materials (Younis et al, 1997) are different from those of the parent rock. Also, the newly formed materials are less massive and less indurated, possessing much lower mechanical strength (Younis et al, 1997). Another possibility is that during erosion processes, some of this new, altered material is broken off, exposing fresh rock. The surfaces of rock outcrops will therefore comprise mixtures of both altered and unaltered material (Mustard and Sunshine, 1999).

4.5 CONCLUSION

Results from continuum removal identified many absorption features for each sample. Possible absorption features were selected based on the literature that was consulted for this study. Since absorption regions may be characteristic for each rock type, it was possible to determine whether statistically significant differences occur in these absorption regions. Statistical analysis was done by running ANOVAs on all wavelengths in the absorption regions. Thereafter, Bonferroni tests were applied to these wavelengths to determine where (comparison between pairs of rocks for all combinations) these significant differences occurred. Here, for each absorption wavelength, for each rock type, comparisons were made against the other remaining rock types to determine which rock type was significantly different from the target rock, e.g. anorthosite, at a particular wavelength, would be significantly different from other rocks, based on their ANOVA values. Also, fresh and weathered samples at each wavelength were analysed and treated as individual samples, due to them having varying spectral properties. There were significant differences between rocks at all absorption wavelengths.

CHAPTER FIVE

RECOMMENDATIONS AND CONCLUSIONS

5.1 INTRODUCTION

Electromagnetic radiation is reflected off natural surfaces at varying intensities. The resultant curve of this measured reflectance depends on numerous variables, such as composition, roughness, particle size and angle of illumination. These variables, specifically composition, influence the shape of the spectral curve and also the position and depth of absorption features. It is within this context that this study determined whether significant spectral differences occurred between rocks samples collected from the ~1145Ma old Mambulu Complex in the northern part of the Natal Belt, South Africa.

5.2 AIMS AND OBJECTIVES REVIEWED

This study aimed to determine whether there were significant spectral differences between rocks of the Mambulu Complex. This was achieved by carrying out the following objectives:

- To capture spectral signatures of the above rock types.

Here, rock samples were brought from the study area to the laboratory for spectral measurements. These measurements were taken under strict lighting and humidity conditions to ensure that the best possible data were collected. Calibrations were done at regular intervals so that measurements were always taken under optimum conditions. Also, samples were rotated after every three measurements to account for the variability in surface roughness.

- To create a spectral library using the collected data.

The spectral data were collected and stored in a spectral library for analysis. The spectral library was created using the ENVI remote sensing software. This software allowed the user to create a library of spectra, which could then be viewed and displayed to the user's specifications. Analytical techniques, such as continuum removal, could also be performed on data held in the spectral library.

- To determine characteristic absorption features for each rock.

Each sample in ENVI is displayed as a spectral curve of wavelength vs. reflectance. The continuum removal method was applied to each spectral curve to enhance absorption features. Using peer-reviewed literature, and knowledge of absorption characteristics, characteristic absorption features were identified for each rock sample. ANOVAs and Bonferroni tests were applied to the wavelengths in each absorption feature to determine if there were spectral differences and between which samples these differences occurred.

5.3 SUMMARY

This reconnaissance study has demonstrated the potential of determining significant spectral differences between rock samples of a layered mafic intrusion, the Mambulu Complex, from the Natal Belt, South Africa. Rock samples collected from the study area were measured in a laboratory. Continuum removal was applied to the spectral data measured from the rock samples. This technique enhanced regions of absorption making it easy to identify absorption features. ANOVAs and Bonferroni tests were run on the wavelengths of these absorption features to determine significant spectral differences and where these occurred. From those results it was evident that significant spectral differences occurred between rocks. These differences were discussed for each absorption feature of every sample type.

5.4 LIMITATIONS OF THIS STUDY

Spectral measurements were only taken under controlled laboratory conditions. No *in situ* measurements were used in this investigation as the location of the study area made it difficult to acquire *in situ* measurements. The area itself, although fairly accessible, was rugged and strewn with loose debris from the Mambulu Complex.

Some absorption features were not considered because they were not distinct or large enough in spectra from the Mambulu Complex. They were, however, considered by other authors (in the literature) based on the effects of transition ions or vibrational processes. These are very complex processes and require sufficient experience and knowledge to infer spectral characteristics from them.

The surface area of the Mambulu Complex is heavily vegetated making lithologic detection very difficult. This impacted negatively on attempts to acquire spectral data, on the Mambulu Complex, from satellite imagery.

The Mambulu Complex may be considered insignificant in terms of its size or contribution to the geological evolution of South Africa. This is itself a limiting factor as not many studies will focus specifically on the Complex, but rather on larger portions of the Natal Belt. Other complexes, such as the Bushveld Complex and the Stillwater Complex, are much larger and more geologically important and are therefore studied in more detail.

5.5 RECOMMENDATIONS

The present study showed that igneous rocks from the same intrusion display significant spectral differences between each other. It focussed solely on determining whether there were significant spectral differences between the rock types of the Mambulu Complex. A few recommendations are proposed for future remote sensing investigations involving the Mambulu Complex and its surrounding areas.

Literature consulted for the study showed that compositional information for rock samples may be derived from field or laboratory spectra. The spectral data collected and the absorption features identified from the rocks from the Mambulu Complex can be used as exploration or mapping tool. This will involve up-scaling (determining diagnostic absorption features) from field and laboratory spectra to hyperspectral imagery. The use of hyperspectral image data presents numerous challenges. Firstly, the image scene must contain rocks of very similar composition to those sampled in situ or in the laboratory. Secondly, these rocks must be sufficiently exposed such that they are identifiable both visually and spectrally in the image. Thirdly, the processing hardware must be able to handle the relatively large amount of data derived from hyperspectral images. It must also be noted that the rocks of the Mambulu Complex were coarse-grained for the most part. Basalt is the fine-grained equivalent of gabbro, and when the spectral signatures of leuco-gabbro from the Mambulu Complex and fine-grained basalt from the JHU spectral library were compared to each other, they were found to have very similar

absorption features. Factors like this need to be considered when using imagery as an exploration or mapping tool.

More in-depth spectral analysis may be performed on the Mambulu spectra. One of these techniques involves a multiple-linear regression of absorption-band parameters (absorption-band position, absorption-band depth and absorption-band asymmetry) and chemical composition (van der Meer, 2004). The absorption band parameter assumes nearly contiguous spectral data. When applied to imaging spectrometer data (discrete spectral bands), van der Meer (2004) proposed the simple linear approximation method of the absorption feature parameters. The above techniques require considerable expertise and experience in spectroscopy.

Absorption features may be used as input to spectral feature fitting techniques that allow for mapping of surface composition/mineralogy from hyperspectral imagery. This process confines the absorption feature analysis to input data in feature fitting. Van der Meer (2004), introduced a linear interpolation method to estimate absorption-band parameters from hyperspectral image data. Absorption feature maps derived using this technique corresponded favourably with the alteration phases that characterized the hydrothermal system studied; and enhanced the analysis of airborne hyperspectral image data for surface compositional mapping (van der Meer, 2004).

Although this study focussed on discriminating and determining significant differences between the spectral signatures of the rocks from the Mambulu Complex, it only touched on the spectral differences between the fresh and weathered surfaces of each of those rock types. The effects of weathering alter both the chemical and mechanical properties of the original material which in turn can significantly change the surface spectral properties of that material (Younis *et al*, 1997). Also taking into account that field measurements involve measurements of exposed surfaces, it is recommended that future remote sensing studies involving the rocks from the Mambulu Complex focus on determining the spectral properties of these fresh and weathered surfaces; and further understanding the effects of weathering on the spectral characteristics of these rock types.

The area covered by the Mambulu Complex is also heavily vegetated and not easily accessible making both *in situ* measurements and remote sensing of this area very difficult. It is, however,

also proposed that future remote sensing studies, in this region, focus on inferring geology from vegetation cover. Since the geology of the complex is already well documented (Bisnath *et al*, 2008; McCourt *et al*, 2006; Bisnath, 2000; Eales *et al*, 1988; and Reynolds, 1984), the chemistry of the underlying rock may be correlated to the type of overlying vegetation. This will require combined knowledge of both remote sensing and geobotany.

5.6 FINAL STATEMENT

Electromagnetic radiation interacts with natural surfaces in a variety of ways. For rocks, these interactions are dependent on composition, particle size, weathering, roughness and atomic interactions. Understanding these interactions and the processes that drive them are crucial to deriving maximum information from spectral data. The applications of ground-based spectroscopy have moved from collecting simple surface measurements to studying the complex subsurface, microscopic relationships between radiation and a variety of surfaces. Both field and laboratory spectroscopy provide a platform to test new technology and techniques for acquiring, processing and analysing spectral data in such a way as to enhance the inferential capacity of image data analysts.

6. REFERENCES

Aarthy, R.S and Sanjeevi, S. (2007). Spectral studies of lunar equivalent rocks – A prelude to lunar material mapping, *Journal of the Indian Society of Remote Sensing*, 35 (2).

Abdel-Rahman, E.M., van den Berg, M., Way, M.J. and Ahmed, F.B. (2009). Handheld spectrometry for estimating thrips (*Fulmekiola serrata*) incidence in sugarcane. *Proceedings of IEEE International Geoscience and Remote Sensing Symposium*, IV-268 – IV-271.

Adam, E. and Mutanga, O. (2009). Spectral discrimination of papyrus vegetation (*Cyperus papyrus L.*) in swamp wetlands using field spectrometry, *ISPRS Journal of Photogrammetry and Remote Sensing*, 64: 612-620.

Anbazhagan, S and Arivazhagan, S. (2010). Reflectance spectra of analog anorthosites: Implications for lunar highland mapping, *Planetary and Space Science*, 58: 752-760.

Anbazhagan, S and Arivazhagan, S. (2011). Characterization of reflectance spectra of lunar analog rocks: gabbro and norite, *Current Science*, 100 (5): 761-768.

Anbazhagan, S, Sainaba, N.K and Arivazhagan, S. (2012). Remote Sensing Study of Sittampundi Anorthosite Complex, India, *Journal of the Indian Society of Remote Sensing*, 40(1):145-153.

ASD (2008). *ViewSpec User Manual*, Analytical Spectral Devices, Inc., Boulder, USA.

Ashwal, L.D. (1993). *Anorthosites*, Spriger-Verlag, Berlin Heidelberg.

Asrar, G. (1989). Introduction, In Asrar, G (Ed). Theory and Applications of Optical Remote Sensing, John Wiley and Sons, New York, p. 1-13.

Bai-Lin, Y. and Xuan, D. (1985). Spectral study of rocks and some iron deposits from Eastern China, *Proceedings of the 3rd International Colloquium on Spectral Signatures of Objects in Remote Sensing 16020 December 1985 (ESA SP-247)*, Les Arcs, France, p. 399.

Bakshi, U.A. and Bakshi, A.V. (2009). *Electromagnetic Wave Theory*, 1st ed, Technical Publications, Pune, India.

Baldridge, A.M., Hook, S.J., Grove, C.I. and Rivera, G. (2009). The ASTER spectral library version 2.0, *Remote Sensing of Environment*, 113: 711-715.

Barker, D.S (1983). *Igneous Rocks*, Prentice Hall, Inc., New Jersey.

Belikov, V.G., Kuregyan, A.G and Ismailova, G.K. (2002). Standardization of Magnetite, *Pharmaceutical Chemistry Journal*, 36 (6): 48-51.

Ben-Dor, E. (2001). Imaging Spectrometry for Urban Applications, In Van der Meer, F. and de Jong, S. Ed. *Imaging Spectrometry: Basic Principles and Prospective Applications*, Kluwer Academic Publishers, 243-280.

Bhatt, M., Mall, U., Bugiolacchi, R., McKenna-Lawlor, S., Banaszkiewicz, M., Nathues, A. and Ullaland, K. (2012). Lunar iron abundance determination using the 2-µm absorption band parameters, *Icarus*, 220: 51-64.

Bisnath, A. (2000). Geology of the Tugela Group rocks in the Nsuze River Valley, Tugela Terrane, Natal Belt, South Africa, M.Sc. Thesis, University of Durban-Westville, South Africa.

Bisnath, A., McCourt, S., Frimmel, H.E and Buthelezi, S.B.N. (2008). The metamorphic evolution of mafic rocks in the Tugela Terrane, Natal Belt, South Africa, *South African Journal of Geology*, 111: 369-386.

Bowden, P., Black, R., Martin, R.F., Ike, E.C., Kinnaird, J.A., & Batchelor, R.A. (1987). Niger-Nigerian alkaline ring complexes: a class example of African Phanerozoic anorogenic mid-plate magnetism. From :Fitton , J.G. & Upton, B.G.J. (eds). Alkaline Igneous Rocks, Geological Society Special Publication No. 30, pp. 357-379.

Campbell, J. B. (2002). *Introduction to Remote Sensing*, Third Edition, The Guilford Press, New York.

Chabrillat, S., Goetz, A.F.H., Krosley, L. and Olsen, H.W. (2002). Use of hyperspectral images in the identification and mapping of expansive clay soils and the role of spatial resolution, *Remote Sensing of Environment*, 82: 431-445.

Christensen, P.R., Bandfield, J.L., Hamilton, V.E., Howard, D.A., Lane, M.D., Piatek, J.L., Ruff, S.W. and Stefanov, W.L. (2000). A thermal emission spectral library of rock-forming minerals, *Journal of Geophysical Research*, 105 (E4): 9735-9739.

Clark, R.N (1999). Spectroscopy of Rocks and Minerals, and Principles of Spectroscopy, In Rencz, A.N. (Ed), *Manual of Remote Sensing*, John Wiley and Sons, New York, 3-58.

Clevers, J.P.G.W. and Jongschaap, R. (2001). Imaging Spectrometry for Agricultural Applications, In Van der Meer, F. and de Jong, S. Ed. *Imaging Spectrometry: Basic Principles and Prospective Applications*, Kluwer Academic Publishers, 157-197.

Cloutis, E.A, Gaffey, M.J, Jackowski, T.L, Reed, K.L. (1986). Calibrations of phase abundance, composition, and particle size distribution of olivine-orthopyroxene mixtures from reflectance spectra, *Journal of Geophysical Research*, 91: 11641-11653.

Cloutis, E.A., Hawthorne, F.C., Mertman, S.A., Krenn, K., Craig., M.A., Marcino, D., Methot, M., Strong, J., Mustard, J.F., Blaney, D.L., Bell III, J.F and Vilas, F. (2006). Detection and discrimination of sulfate minerals using reflectance spectroscopy, *Icarus*, 184: 121-157.

Cloutis, E.A., Klima, R.L., Kaletzke, L., Coradini, A., Golubeva, L.F., McFadden, L.A., Shestopalov, D.I., Vilas, F. (2010). The 506nm absorption feature in pyroxene spectra: Nature and implications foor spectroscopy-based studies of pyroxene-bearing targets, *Icarus*, 207: 295-313.

Cracknell, A.P. and Hayes, L. (1991). *Introduction to Remote Sensing*, Taylor and Francis Ltd, London.

Curtiss, B. and Goetz, A.F.H. (1999). *Field Spectrometry: Techniques and Instrumentation*, ASD Technical Field Guide 3rd Ed, Section 12, Analytical Spectral Devices, Inc., Boulder, USA.

Debba, P., van Ruitenbeek, F.J.A., van der Meer, F.D., Carranza, E.J.M., Stein, A. (2005). Optimal field sampling for targeting minerals using hyperspectral data, *Remote Sensing of Environment*, 99: 373-386.

Deering, D.W. (1989). Field Measurements of Bidirectional Reflectance, In, Theory and Applications of Optical Remote Sensing, Asrar, G (Ed). Chapter 2, p. 14-65.

Demattê, J.A.M., Campos, R.C., Alves, M.C., Fiorio, P.R and Nanni, M.R. (2004). Visible-NIR reflectance: a new approach on soil evaluation, *Geoderma*, 121: 95-112.

Department of Mineral Resources (2011). *A Beneficiation Strategy for the Minerals Industry of South Africa*, Department of Mineral Resources, Republic of South Africa.

Eales, H.V., Wilson, A.H. and Reynolds, I.M. (1988). Complex unmixed spinels in layered intrusions within an obducted ophiolite in the Natal-Namaqua mobile belt, *Mineralium Deposita*, 23: 150-157.

Elachi, C. and Van Zyl, J. (2006). *Introduction to the physics and techniques of remote sensing*, John Wiley and Sons, Inc, New Jersey.

ENVI (2009). Environment for Visualising Images, Release 4.7, ITT Visual Information Solutions, ITT Industries Inc., USA.

Goetz, A.F.H (1985). Imaging Spectrometry for Earth Remote Sensing, *Science*, 228 (4704): 1147-1153.

Goetz, A.F.H (1989). Spectral Remote Sensing in Geology, In, Theory and Applications of Optical Remote Sensing, Asrar, G (Ed). Chapter 12, p. 491-526.

Gomez, C., Lagacherie, P. and Coulouma, G. (2008). Continuum removal versus PLSR method for clay and calcium carbonate content estimation from laboratory and airborne hyperspectral measurements, *Geoderma*, 148: 141-148.

Gupta, R.P. (1991). Remote Sensing Geology, Springer-Verlag, Berlin.

Hauff, P. (no date). An Overview of VIS-NIR-SWIR Field Spectroscopy as Applied to Precious Metals Exploration, Spectral International Inc., Arvada, Colorado.

Hatchell, D. (1999). *Reflectance*, ASD Technical Field Guide 3rd Ed, Section 17, Analytical Spectral Devices, Inc., Boulder, USA.

Herold, M., Roberts, D.A., Gardner, M.E. and Dennison, P.E. (2004). Spectrometry for urban area remote sensing – Development and analysis of a spectral library from 350 to 2400nm, *Remote Sensing of Environment*, 91: 304-319.

Johnston, S.T., McCourt, S., Bisnath, A. and Mitchell, A.A. (2003). The Tugela Terrane, Natal belt: Kibaran magmatism and tectonism along the southeast margin of the Kaapvaal Craton, *South African Journal of Geology*, 106: 85-97.

Kalacska, M., Bohlman, S., Sanchez-Azofeifa, G.A., Castro-Esau, K. and Caelli, T. (2007). Hyperspectral discrimination of tropical dry forest lianas and trees: Comparative data reduction approaches at the leaf and canopy levels, *Remote Sensing of Environment*, 109: 406-415.

Kaufmann, H., Segl, K., Itzerott, S., Bach, H., Wagner, A., Hill, J., Heim, B., Opperman, K., Heldens, W., Stein, E., Muller, A., van der Linden, S., Leitao, P.J., Rabe, A and Hostert, P. (2010). *Hyperspectral algorithms: report of the frame of EnMap preparation activities*, Scientific Technical Report STR10/08, Postdam.

Kearney, L. (2012). *Mining and Minerals in South Africa*, SouthAfrica.info, Brand South Africa, [www.southafrica.info Accessed: 14 October 2012].

Kuzvart. M. and Bohmer, M. (1986). Prospecting and exploration of mineral deposits, Developments in economic geology 21, Elsevier, Amsterdam.

Lagacherie, P., Baret, F., Feret, J.B., Netto, J.M. and Robbez-Masson, J.M. (2008). Estimation of soil clay and calcium carbonate using laboratory, field and airborne hyperspectral measurements, *Remote Sensing of Environment*, 112: 825-835.

Le Maitre, R.W. (Ed). (2004). *Igneous Rocks: A Classification and Glossary of Terms*, 2nd, Cambridge University Press, United Kingdom.

Lewis, D.W. and McConchie, D. (1994). Practical Sedimentology, Second Edition, Chapman and Hall, New York.

Liese, H.C. (1967). An Infrared Absorption Analysis of Magnetite, *The American Mineralogist*, 52: 1198-1205.

Linstrom, W. (1987). *The Geology of the Dundee Area, Geological Survey*, Department of Mineral and Energy Affairs, Republic of South Africa.

MacKenzie, W.S., Donaldson, C.H. and Guilford, C. (1982). *Atlas of igneous rocks and their textures*, Halsted Press, United States of America.

Malenovsky, Z, Bartholomeus, H.M, Acerbi-Junior, F.W, Schopfer, J.T, Painter, T.H, Epema, G.F, Bregt, A.K. (2007). Scaling dimensions in spectroscopy of soil and vegetation, *International Journal of Applied Earth Observation and Geoinformation*, 9: 137-164.

Mather, P and Koch, M (2011). Computer Processing of Remotely-Sensed Images: An Introduction, 4th Edition, John Wiley & Sons, Chichester.

Matthews, P.E and Charlesworth, E.G (1981). *A geological review of the Northern margin of the Proterozoic Namaqua-Natal Mobile Belt in Natal*, Guide-book to the post-congress excursion to Natal, Geocongress, Pretoria, Geological Society of South Africa.

McCourt, S., Armstrong, R.A., Grantham, G.H., Thomas, R.J. (2006). Geology and evolution of the Natal belt, South Africa, *Journal of African Earth Sciences*, 46: 71-92.

Mehta, S. (1985). Radiometric Data Characterise Quantisation of Soil Forming Minerals, *Proceedings of the 3rd International Colloquium on Spectral Signatures of Objects in Remote Sensing 16020 December 1985 (ESA SP-247)*, Les Arcs, France, p. 249.

Meroni, M., and Colombo, R. (2009). 3S A novel program for field spectroscopy, *Computers and Geoscience*, 35 (7): 1491-1496.

Middlemost, E.A.K. (1985). *Magmas and Magmatic Rocks: An introduction to igneous petrology*, Longman Inc, New York.

Milton, E.J., Schaepman, M.E., Anderson, K., Kneubuhler, M., Fox, N. (2009). Progress in field spectroscopy, *Remote Sensing of Environment*, 113: S92-S109.

Moroz, L.V, Basilevsky, A.T, Hiroi, T, Rout, S.S, Baither, D, van der Bogert, C.H, Yakovlev, O.I, Fisenko, A.V, Semjonova, L.F, Rusakov, V.S, Khramov, D.A, Zinovieva, N.G, Arnold, G, and Pieters, C.M. (2009). Spectral properties of simulated impact glasses produced from martian soil analogue JSC Mars-1, *Icarus*, 202: 336-353.

Mustard, J. F and Sunshine, J.M (1999). Spectral Analysis for Earth Science: Investigations Using Remote Sensing Data. In Rencz, A.N. Ed. *Remote Sensing for the Earth Sciences: Manual of Remote Sensing*, John Wiley & Sons, Inc. 251-306.

Mutanga, O., Skidmore, A.K. and Prins, H.H.T. (2004). Predicting in situ pasture quality in the Kruger National Park, South Africa, using continuum-removed absorption features, *Remote sensing of Environment*, 89: 393-408.

Nicodemus, F.E, Richmond, J.C., Hsia, J.J, Ginsberg, I.W. and Limperis, T.L. (1977). Geometrical considerations and nomenclature for reflectance. National Bureau of Standards Monograph, 160: 20402.

Noomen, M.F., Skidmore, A.K., van der Meer, F.D. and Prins, H.H.T. (2006). Continuum removed band depth analysis for detecting the effects of natural gas, methane and ethane on maize reflectance, *Remote Sensing of Environment*, 105: 262-270.

O'Connell, R.W. (2012). Electromagnetic Waves, Astronomy 1210: Supplement III, University of Virginia, [http://www.astro.virginia.edu/class/oconnell/astr121/121supps2-3.html. Accessed: 15 May 2012].

Oliff, W.D. (1960). Hydrobiological studies on the Tugela river system, *Hydrobiologia*, 14 (3-4): 281-332.

Palacios-Orueta, A and Ustin, ,S.L. (1996). Multivariate Statistical Classification of Soil Spectra, *Remote Sensing of Environment*, 57: 108-118.

Pompilio, L., Sgavetti, M and Pedrazzi, G. (2007). Visible and near-infrared reflectance spectroscopy of pyroxene-bearing rocks: New constraints for understanding planetary surface compositions, *Journal of Geophysical Research*, 112 (E01004):1-23.

Qaid, A.M, Basavarajappa, H.T and Rajendran, S. (2009). Integration of VNIR and SWIR Spectral Reflectance for Mapping Mineral Resources; A Case Study, North East of Hajjah, Yemen, *Journal of Indian Society of Remote Sensing*, 37:305-315.

Raja, S, Rajendran, S, Poovalinga Ganesh, B and Thirunavukkarasu, A (2010). Study on Hyperspectral Signatures for Magnetite Iron ore in Thattayengerpet Region of Trichirappalli District in Tamil Nadu State, India, *International Journal of Geomatics and Geosciences*, 1(2): 188-196.

Rajesh, H.M. (2004). Application of remote sensing and GIS in mineral resources -An overview, *Journal of Mineralogical and Pedological Sciences*, 99: 83-103.

Reynolds, I. M. (1984). Tectonically deformed ilmenite in titaniferous iron ores of the Mambula Complex, Zululand, South Africa, *Canadian Mineralogist*, 22: 411-416.

Schaepman, M.E., Ustin, S.L., Plaza, A.J., Painter, T.H., Verrelst, J. and Liang, S. (2009). Earth system science related imaging spectroscopy – An assessment, *Remote Sensing of Environment*, 113: S123-S137.

Schaepman-Strub, G., Schaepman, M.E., Painter, T.H., Dangel, S. and Martonchik, J.V. (2006). Reflectance quantities in optical remote sensing – definitions and case studies, *Remote Sensing of Environment*, 103: 27-42.

Schmidt, K.S and Skidmore, A.K (2003). Spectral discrimination of vegetation types in a coastal wetland, *Remote Sensing of Environment*, 85: 92-108.

Sgavetti, M., Pompilio, L. and Meli, S. (2006). Reflectance spectroscopy (0.3-2.5µm) at various scales for bulk-rock identification, *Geosphere*, 2(3): 142-160.

SPSS (2010). *IBM SPSS Statistics 19*, Statistical Package for the Social Sciences, SPSS Inc., Chicago, USA.

Van der Meer, F. (2001). Basic Physics of Spectrometry. In Van der Meer, F. and de Jong, S. Ed. *Imaging Spectrometry: Basic Principles and Prospective Applications*, Kluwer Academic Publishers, 3-16.

Van der Meer, F., de Jong, S. and Bakker, W. (2001). Imaging Spectrometry: Basic Analytical Techniques. In Van der Meer, F. and de Jong, S. Ed. *Imaging Spectrometry: Basic Principles and Prospective Applications*, Kluwer Academic Publishers, 17-61.

Van der Meer, F. (2004). Analysis of spectral absorption features in hyperspectral imagery, *International Journal of Applied Earth Observation and Geoinformation*, 5:56-68.

Wester, K. and Lunden, B. (1985). Laboratory Measurements of Spectral Reflectance (0.4-2.3µm) of Basalts, *Proceedings of the 3rd International Colloquium on Spectral Signatures of Objects in Remote Sensing 16020 December 1985 (ESA SP-247)*, Les Arcs, France, p. 523.

Younis, M.T., Gilabert, M.A., Melia, J. and Bastida, J. (1997). Weathering process effects on spectral reflectance of rocks in a semi-arid environment, *International Journal of Remote Sensing*, 18 (16): 3361-3377.

Zeng, Y., Bartholomeus, H.M., De Bruin, S., Epema, G.F., Clevers, J.G.P.W. (2003). Using hyperspectral remote sensing data for identifying geological and soil units in the Alora Region, Southern Spain, *3rd EARSeL Workshop on Imaging Spectroscopy*, Herrsching.